

國立交通大學

電控工程研究所

碩士論文

禪坐者之心肺相位同步分析

Cardiorespiratory phase synchronization

for Chan-meditation practitioners



研究生：黃順敏

指導教授：羅佩禎 博士

中華民國九十九年七月

禪坐者之心肺相位同步分析

Cardiorespiratory phase synchronization
for Chan-meditation practitioners

研究生：黃順敏

Student : Shun-Min Huang

指導教授：羅佩禎 博士

Advisor : Dr. Pei-Chen Lo

國立交通大學



Submitted to Institute of Electrical and Control Engineering
College of Electrical Engineering National Chiao Tung University

In Partial Fulfillment of the Requirements

For the Degree of

Master

In

Electrical and Control Engineering

July 2010

Hsinchu, Taiwan, Republic of China

中華民國九十九年七月


禪坐者之心肺相位同步分析

研究生：黃順敏

指導教授：羅佩禎 博士

國立交通大學電控工程研究所

摘要



本研究主要是想探討禪坐練習者在不同的呼吸速率下，心肺交互作用的情形，我們用心率時間序列和呼吸訊號的瞬時相位去觀察此一現象，由於心率的變化是由很多不同的生理機制所影響，故使用傳統的線性方法很難準確的估算心率時間序列的瞬時相位，故本研究使用希爾伯特-黃轉換去分析心率時間序列，它是近來被用來處理非線性訊號的方法，我們希望藉由希爾伯特-黃轉換去獲得更為準確的瞬時相位。本研究共收集了12年齡相似的受測者的心電圖和呼吸訊號，其中實驗組為6具有禪坐經驗者，而控制組6受測者則無此經驗。由結果發現，控制組在控制呼吸為每分鐘10次的實驗階段有顯著性($p < 0.02$)心肺相位同步現象發生，而實驗組所呈現的結果相較於控制組是較分歧的。我們假設主要的原因為實驗組在禪定過程中的呼吸率是不一致的，禪定者的呼吸率會隨著時間而一直變化著。根據此結果，我們推論在比較慢並且變化比較平穩的呼吸速率下，可能會增加心肺系統之間的同步現象。

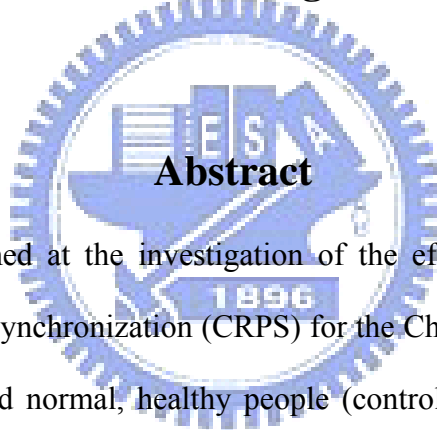
Cardiorespiratory phase synchronization for Chan-meditation practitioners

Student : Shun-Min Huang

Advisor :Dr. Pei-Chen Lo

Institute of Electrical and Control Engineering

National Chiao Tung University



Abstract

This research is aimed at the investigation of the effect of respiratory rate on cardiorespiratory phase synchronization (CRPS) for the Chan-meditation practitioners (experimental group) and normal, healthy people (control group). Cardiorespiratory phase synchronization was evaluated by the instantaneous phase of the heart-rate (HR) sequence and respiratory signal. Conventional linear method cannot provide a reliable estimate of instantaneous phase of HR sequence due to the possible interference of other biological artifacts to the HR activities. To deal with the issue, Hilbert-Huang transform (HHT) was adopted to decompose HR sequence. HHT has been applied to nonlinear signal processing recently. We aimed to attain a more precise estimate of instantaneous phase by HHT scheme. In this study, ECG (electrocardiograph) signals and respiratory signals of twelve subjects were recorded. Among them, six subjects were Chan-meditation practitioners and the other six subjects are normal people in the same age range, yet, without any meditation experience. The control group was

requested to follow intentionally designed protocol in the recording, while the experimental subjects only practiced Chan meditation. In our preliminary results, control subjects exhibited significant better degree of CRPS in the session of breathing control at the rate of 10 breaths/min. On the other hand, experimental group did not exhibit significant correlation between CRPS and respiratory rate. According to the time-dependent respiratory signal, meditation practitioners breathed in a free style during Chan meditation and thus could not keep a constant respiratory rate for a moderate duration. The experimental group thus did not achieve the state of CRPS as good as the control group even at the same respiratory rate of 10 breaths/min. We thus make an assumption that a consistently slow respiration can induce an efficient CRPS.



誌 謝

二年很快的過去了，我畢業了！先感謝電控所的教授們有這麼多豐富的課程得以修習，令我在專業知識上獲益良多。

家人是我最重要的依靠—爸、媽、姊姊、哥哥以及堂哥，可以持續求學，都是因為你們的支持和體諒，你們是我最大的靠山。

我最美麗的指導教授—羅佩禎博士，感謝您在學術研究上的身教、言教。以前的我總是缺乏自信，而您總是給我很多學習的機會，讓我覺得自己也可以完成許多事，增加我對自己信心。您是我生命中的貴人。

可愛的實驗室助理們—意屏總是在 meeting 時準備好吃的點心。洵好讓實驗室的網頁煥然一新。瑋婷在研究上的幫忙。

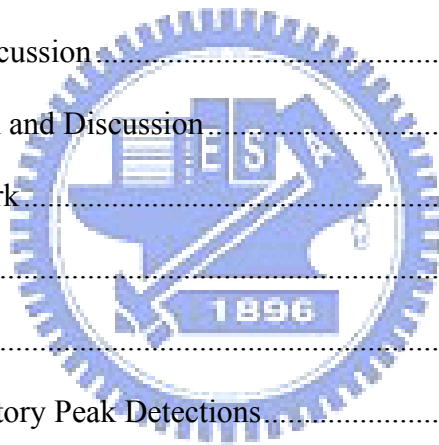
研究路上的戰友們—適達幫我建立了很多 DSP 的觀念。家鈞陪我挑燈夜戰。淮璋和我一起抱怨網路程式設計那群機車的助教。銓懋總是貼心的提醒我一些學校的大小事。最講義氣的明誠、宣胖和仁宏每次都排除萬難的陪我打球。實驗室的衛星導航翔宇和介均，有你們兩個要迷路根本就是不可能。

最後，感謝口試委員—張剛鳴教授、林國瑞教授，有您的指導，我的碩士論文才能更臻完備。

Content

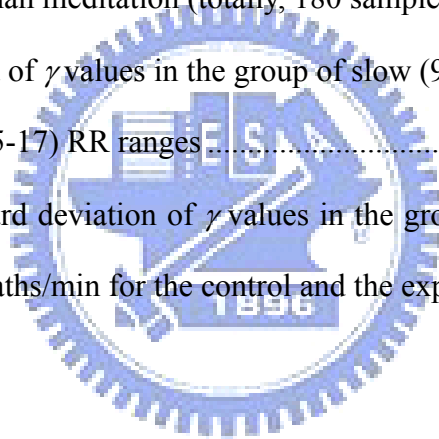
Content.....	i
List of Tables.....	iii
List of Figures.....	iv
Chapter1.....	1
Introduction.....	1
1.1 Background and Motivation.....	1
1.2 Aim of this work.....	3
Chapter 2.....	4
Theories and Methods.....	4
2.1 Introduction to ECG and Respiration.....	5
2.1.1 Introduction to ECG.....	5
2.1.2 Chest and Abdominal Respiration.....	8
2.2 Instantaneous phase analysis.....	10
2.2.1 Introduction to HHT.....	10
2.2.2 Empirical Mode Decomposition (EMD) method.....	13
2.2.3 Discrete Hilbert transform (DHT).....	18
2.3 Analysis of Cardiorespiratory Phase Synchronization.....	19
Chapter 3.....	23
Experiment and Signal Analysis.....	23
3.1 Experimental Setup and Procedure.....	23
3.1.1 Control Group.....	24
3.1.2 Experimental Group.....	24
3.1.3 Signal Acquisition.....	25

3.1.4	Measurement of ECG signal.....	27
3.1.5	Measurement of respiratory signal	28
3.2	Cardiorespiratory Phase Synchronization Analysis.....	29
3.3	Strategy for Estimating Respiratory Rate	35
Chapter 4	36
Results and Inspection	36
4.1	Results for control group	36
4.2	Results for experimental group.....	43
4.3	Overall comparison between two groups.....	54
Chapter 5	59
Conclusion and Discussion	59
5.1	Conclusion and Discussion.....	59
5.2	Future Work.....	60
Reference	61
Appendix A	65
R Peak and Respiratory Peak Detections.....		65
I.1	R Peak Detection	65
I.2	Respiratory Peak Detection	67
Appendix B	70
Formal Chan-meditation Practice		70
Appendix C	71
Continuous Hilbert transform		71



List of Tables

2.1	Described each ECG complex correlates to the particular task of the cardiac cycle	7
2.2	Comparison among STFT, wavelet, and HHT analysis.....	12
3.1	Subjects of experimental and control groups.....	23
4.1	RR ranges of slow, medium, and fast breathing for each individual subject in the experimental group (Chan-meditation practitioners).....	48
4.2	Number of samples within each RR range for all six experimental subjects under 30-minute Chan meditation (totally, 180 samples).....	51
4.3	The average and std of γ values in the group of slow (9-11), medium (12-14), and fast (15-17) RR ranges.....	53
4.4	Average and standard deviation of γ values in the group of RR's: <8, 8-12, 12-16, and >16 breaths/min for the control and the experimental group	57



List of Figures

2.1	The conducting system of the human heart.....	6
2.2	The standard wave pattern of ECG	7
2.3	Illustration of expiration and inspiration mechanisms in chest respiration	9
2.4	Illustration of expiration and inspiration mechanisms in abdominal breathin.....	9
2.5	Flow chart for EMD.....	16
2.6	An ideal time series $x[n]$ simulated by three sinusoidal components	17
2.7	First four IMF components of $x[n]$	17
2.8	Examples for cardiorespiratory desynchronization (left column) and synchronization (right column).....	22
3.1	Experimental procedure for the control group. Four sessions include (1) baseline measurement (5 minutes), (2) breath control at 10 breaths/min (10 minutes), (3) breath control at 6 breaths/min (10 minutes), and (4) post-test natural breathing (5 minutes).....	24
3.2	Physiological signal recording system: (a) Bio-amplifiers, and (b) digitization and on-line monitoring system.	26
3.3	Physiological signal recording system for experimental group: (a) Bluetooth Bio-amplifiers, and (b) digitization and on-line monitoring system.....	26
3.4	(a) ECG electrode, and (b) Bipolar limb-lead II electrode placement(experimental group) and (c) Biopolar limb-lead I electrode placement(control group).....	27
3.5	Piezo-electric respiratory transducer.....	28
3.6	Respiratory signal	28

3.7	Flow chart for the strategy for analyzing the cardiorespiratory phase synchronization.....	29
3.8	Flow chart for the strategy for estimating the instantaneous phase of (a) HR and (b) RP sequences.....	31
3.9	The first four IMF components $c_i[n]$, $i=1-4$ of the <i>HR</i> time series for control subject #5.....	32
3.10	The 30-minute cardiorespiratory phase difference scenario for experimental subject #3.....	33
3.11	Running-window scheme used to assess the temporal evolution of degree of cardiorespiratory phase synchronization.....	33
3.12	Degree of phase synchronization γ (experimental subject #3) evaluated with the running-window scheme (size 1 minute, moving step 10 seconds).....	34
3.13	Time-varying respiratory rate analyzed for experimental subject #3.....	35
4.1	Analysis of cardiorespiratory phase synchronization for control group. (a)-(f) are the results for control subjects #1 to #6, respectively. Results include 1) time-dependent phase difference ψ , 2) time-dependent <i>dps</i> γ , and 3) ψ histogram.....	37
4.2	Monochrome image representation of the 30-min <i>dps</i> γ for all six control subjects.....	40
4.3	Average <i>dps</i> in each session for control subjects #1 to #6.....	41
4.4	Average <i>dps</i> of all 6 control subjects in the same session. The symbol ** denotes significant difference ($p<0.02$) justified by t-test existing between the second session and the other sessions.....	42
4.5	Monochrome image representation of the 30-min <i>dps</i> γ for all six experimental subjects.....	44

4.6 RR histograms for each meditation practitioner during the entire Chan-meditation course	45
4.7 Heart-rate histograms for each meditation practitioner during the entire Chan-meditation course	46
4.8 The dps (γ) histogram for each meditation practitioner during the entire Chan-meditation course	47
4.9 The γ histograms corresponding to the slow (left), medium (middle), and fast (right) respiratory ranges for experimental subjects #1 to #6 in (a) to (f).	49
4.10 Bar-chart illustration of the average and std of γ values in the slow, medium, and fast RR ranges for each experimental subject.	50
4.11 The time-dependent Respiratory rate for experimental subject.	52
4.12 RR histogram for all the control subjects. There will be totally $180 \times 6 = 1080$ R samples.	54
4.13 RR histogram for all the experimental subjects (1080 RR samples overall).	54
4.14 The γ distributions with the RR in the range (from the top): <8 , 8-12, 12-16, and >16 breaths/min for the control group.	55
4.15 The γ distributions with the RR in the range (from the top): <8 , 8-12, 12-16, and >16 breaths/min for the experimental group.	56
4.16 Average of γ values in the group of RR's: <8 , 8-12, 12-16, and >16 breaths/min for the control and the experimental group.	58
A.1 Flow chart of R peak detection.	66
A.2 The raw ECG and preprocessed ECG.	67
A.3 Flow chart of Respiratory peak detection	68
A.4 The raw and preprocessed respiratory signal	68
A.5 Parameters for respiratory signal peak detection.	69

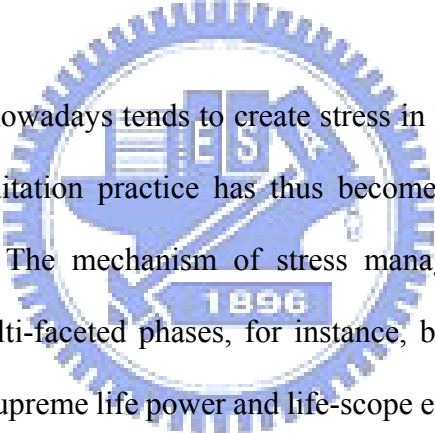
Chapter1

Introduction

1.1 Background and Motivation

Meditation nowadays is widely acknowledged as one important technique in the category of mind-body medicine after having been proved to benefit human health and wellness in various aspects via the extensive, profound researches since 1960s[1][2] and Meditation is described as a wakeful hypometabolic state of parasympathetic dominance that has been corroborated by such physiological indicators as the reduction of heart rate, blood pressure, and respiratory rate, significant increase in plasma melatonin levels and better regulation of cortisol level[3][4][5]. Among various meditation techniques, Chan meditation originating from Dharma-Chan reveals an extraordinarily unique way of practicing meditation via “holy-heart unification” enlightenment. Our previous study on EEG (electroencephalograph) has revealed some exclusive characteristics of a Chan-enlightened brain [6][7]. Nevertheless, the core doctrine in Dharma Chan focuses a great deal on the practice of *heart* purification that has been assumed to power the Chan-enlightened brain. Mechanism of heart purification involves both Chan wisdom practice and heart-chakra purification. Chan-meditation practitioners thus have been experiencing various evolutionary states of heart perception that inspires us to investigate the cardiac physiology during Chan meditation. To the best of our knowledge, no study has been reported on the cardiorespiratory interaction during Chan-meditation practice because orthodox Dharma-Chan practice is rarely found in the current era.

Cardiorespiratory phase synchronization (CPRS) is a recently investigated phenomenon reflecting certain type of interaction between cardiac and respiratory systems. According to previous studies[8][9], cardiorespiratory phase synchronization may establish an effectual co-action between cardiac and respiratory systems which can preserve the body energy. Cardiorespiratory phase synchronization was most visible under conditions of low cognitive activity, such as during sleep[8][10] and anesthesia[11][12], and was almost lost during physical strain[8]. The transcendental-consciousness state during meditation is a condition of low cognition level. According to previous studies, it may facilitate the appearance of CPRS.



The living manner nowadays tends to create stress in varying degrees and forms for modern people. Meditation practice has thus become one of the most popular stress-relief approaches. The mechanism of stress management via Dharma-Chan meditation involves multi-faceted phases, for instance, bioenergy enhancement via harmonizing with Chan supreme life power and life-scope expansion via Chan wisdom enlightenment. In our previous study on stress scale survey on Taiwan college students, we observed the substantial effect of Chan meditation on stress manipulation and emotion regulation[13]. Cardiorespiratory interaction has been identified as an important index of health condition and stress-management ability. Moreover, cardiorespiratory function can be assessed quantitatively by simultaneously recording ECG (electrocardiograph) and respiratory signals.

1.2 Aim of this work

Breathing regulation to calm down the mind and mood is one of the most important fundamentals of Chan meditation for the beginners. In addition, correct breathing trained by meditation helps one to better manage the body and mind stress and therefore to enhance the health state and living quality. These advantages inspired us to investigate the relationship between cardiorespiratory interaction and respiratory rates. In this thesis, we studied the cardiorespiratory interaction scheme based on the analysis of instantaneous phases of heart-rate time series and raw respiratory signal.



Chapter 2

Theories and Methods

According to Chan-Meditation practitioners, perceived benefits to health have been confirmed in the physiological, psychological, behavioral, and mental aspects. Researchers accordingly intended to investigate the phenomena of meditation as early as in the 1950's. Scientific evidences based on measurable, empirical data have been reported at an increasing rate, thanks to the fast development of sophisticated medical instruments that provide the media for gaining access to physiological signals. Nevertheless, we hardly found any report of the effects of Chan-meditation practice on cardio-respiratory interaction that has been identified as an important index of health condition and stress-management ability. The cardiorespiratory function now can be assessed quantitatively by simultaneously recording ECG (electrocardiograph) and respiratory signals.

Scientific researches have demonstrated that a number of physiological signals accessible noninvasively significantly reveal the normal/abnormal and physically/mentally health states of human body. They even have become routinely clinical reference or medical-checkup items due to the ease of implementation. Examples of these physiological signals include ERP (evoked-response potential), EMG (electromyograph), ECG, GSR (galvanic Skin Response), and respiratory signal.

2.1 Introduction to ECG and Respiration

2.1.1 Introduction to ECG

As the core organ of the circulatory system, human heart pulsates automatically and rhythmically. Such mechanical activity is manipulated by a specialized conducting system composed of SA node (sinoatrial node), AV node (atrioventricular node), Bundle of His, and Purkinje fibers as shown in Fig.2.1. Pacemaker cells in SA node depolarize at the rate of approximately 72 times per minute to control the rhythmic pulsation of heart. The depolarization waves (action potential) spread out through the atria and propagate via the particular conduction pathways till reaching the cells of ventricles. When action potential travels to atria, atrial cells depolarize that causes the contraction of atria and results in the so-called P wave in ECG. After transmitting through AV node, Bundle of His, and Purkinje fibers (the extended part of the fibers of Bundle of His), action potential finally spreads to ventricular cells. The depolarization of ventricular cells causes the action of ventricular systole, which is recorded as the QRS wave (or simply R wave) in ECG. Then, T wave appears as the ventricular cells repolarize (ventricular diastole). Note that the wave of atrial repolarization is masked by the dominant QRS during ventricular depolarization. In sum, the electrical-conduction mechanism driving the atrial and ventricular, mechanical systole/diastole rhythms follows the sequence: SA node → atria → AV node → Bundle of His → Purkinje fibers → ventricles[14].

The depolarization waves not only induce the mechanical pumping of heart but also generate the variation of electrical potential on the body surface that is recordable noninvasively. ECG is the signal revealing such electrical-potential change. Without stimulation, the heart cells are in the quiescent state (-80 mV or so) with negative potential (so-called polarization). After stimulation, they bear positive potential which induces the systole reaction. Hence, ECG traces the potential variation of periodic activity of the heart.

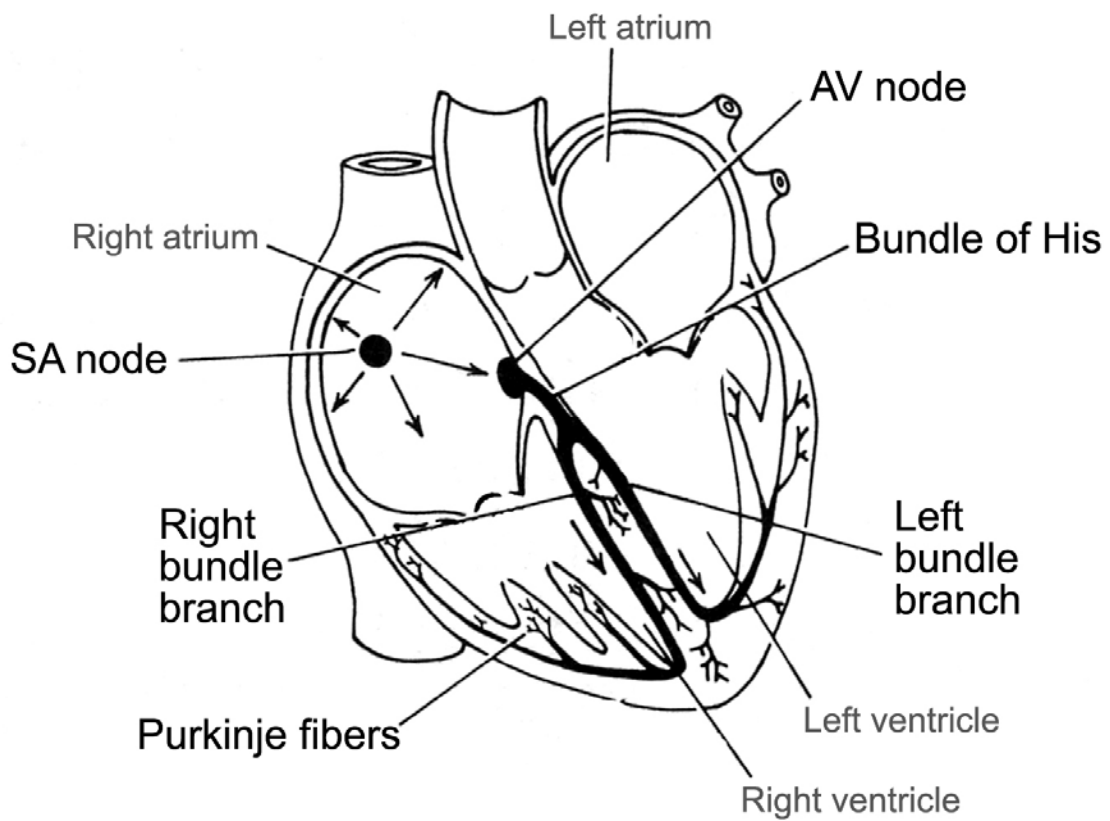


Fig 2. 1 The conducting system of the human heart. [14]

Table 2. 1 Described each ECG complex correlates to the particular task of the cardiac cycle.

ECG pattern	Electrical activity	Mechanical activity
P wave	Depolarization of atrial cells	Atrial contraction
QRS complex	Depolarization of ventricular cells	Ventricular contraction
T wave	Repolarization of ventricular cells	Ventricular expansion

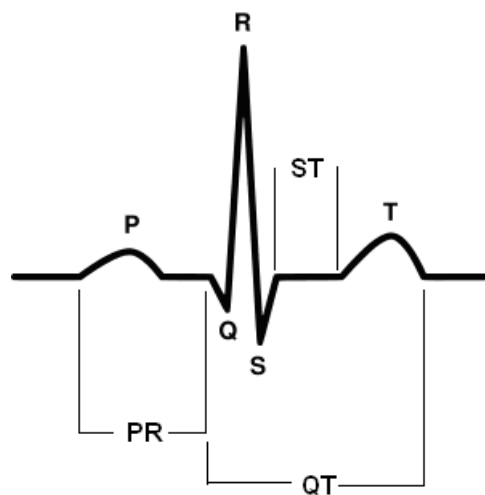


Fig 2. 2 The standard wave pattern of ECG

2.1.2 Chest and Abdominal Respiration

The respiration provides a means of acquiring oxygen and eliminating carbon dioxide for survival. The mechanism of respiration involves the muscular motions that change the volume of the thoracic cavity to achieve gas exchange by inspiration (inhalation) and expiration (exhalation). Normal, chest respiration is accomplished by two sets of muscles, the diaphragm and intercostal muscles. They operate together to carry out the task of inhalation/exhalation. On the other hand, abdominal respiration having been recognized to be a much healthier respiration manner is accomplished mainly by the abdominal muscles and diaphragm.

The diaphragm, capable of moving up and down, is the wall that separates the abdomen from the thoracic cavity. The intercostal muscles together with the ribs form the thoracic cavity and move the rib cage in and out. As shown in Fig.2.3, normal expiration is resulted from the integration of the upward motion of diaphragm and the inward swing of rib cage. Hence, the reduced cavity housing the lungs results in a pressure increase of -3mm Hg with respect to the pressure outside the body. Accordingly, air flows out of the lungs that completes the expiration scheme. On the contrary, inspiration follows the reverse mechanism.

In abdominal breathing, abdominal muscles expand causing the downward movement of diaphragm and, consequently the increase of thoracic-cavity volume inducing the air in (inspiration). While during the expiration, contraction of abdominal muscles moves diaphragm upward and narrow the thoracic-cavity volume that results in the air-out action. Instrumentation with appropriate transducer can be adopted to record the respiration activities by transforming mechanical energy into electrical energy (for example, strain gauge).

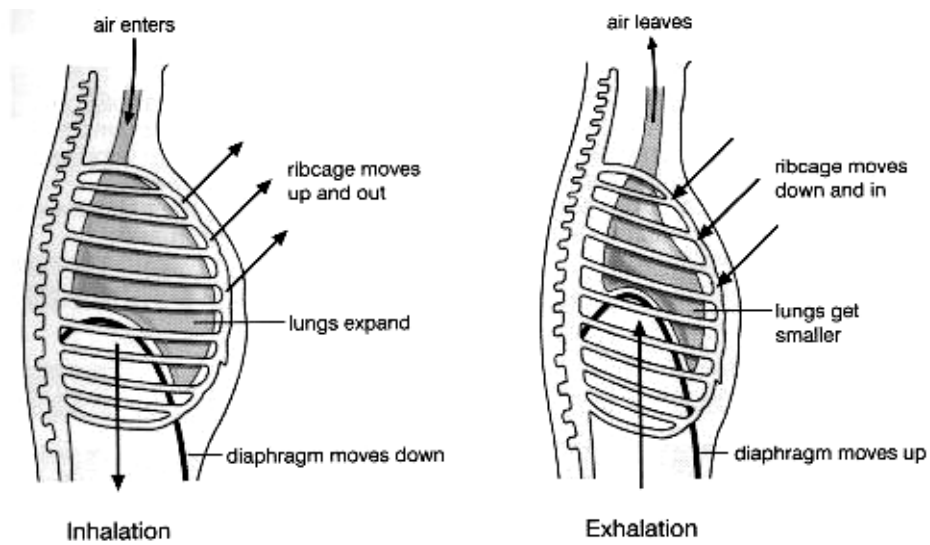


Fig 2. 3 Illustration of expiration and inspiration mechanisms in chest respiration

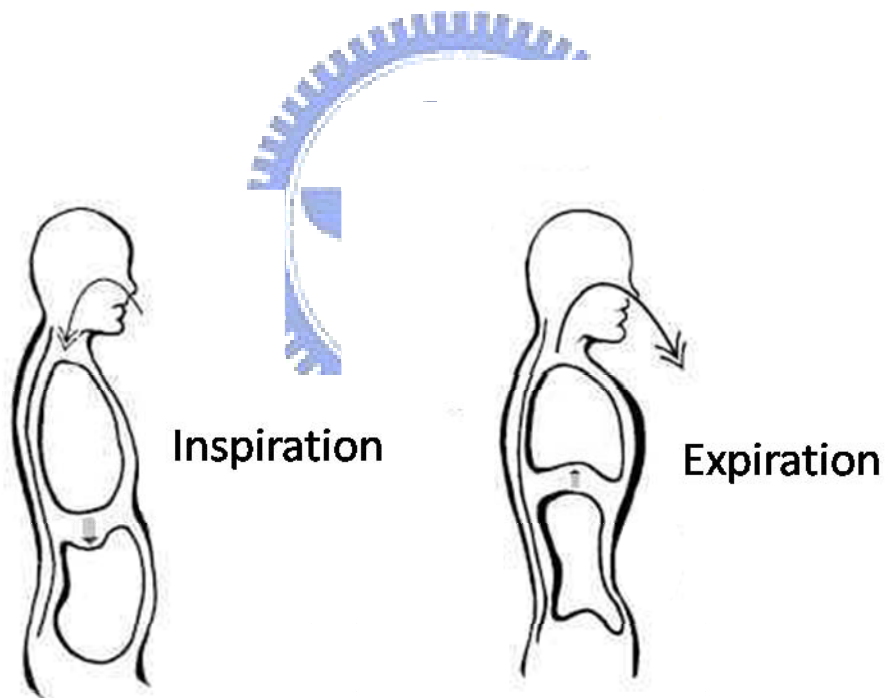


Fig 2. 4 Illustration of expiration and inspiration mechanisms in abdominal breathing

2.2 Instantaneous phase analysis

A number of methods have been proposed to evaluate the phase synchronization phenomenon between two possibly coupled oscillatory systems (reference). However, Like almost all natural phenomena, HRV is the result of many nonlinearly interacting processes; therefore any linear analysis has the potential risk of underestimating, or even missing, a great amount of information content. Accordingly, we applied the instantaneous phase analysis based on Hilbert-Huang Transform (HHT) to our study of cardiorespiratory interaction properties for Chan-meditation practitioners and controls. The following sections introduce the theory, method and implementation scheme.

2.2.1 Introduction to HHT

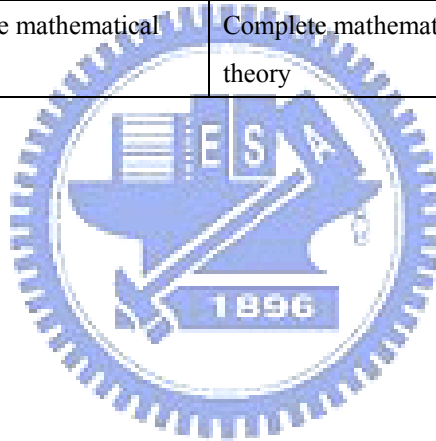
Conventional methods for frequency and phase analysis are mostly based on linear and stationary assumptions. Only in recent years have researchers begun to analyze the rhythmic behaviors from the view of nonstationary and nonlinearity. For example, wavelet analysis and the Wagner-Ville distribution [15][16] were designed for linear but nonstationary data. Additionally, various nonlinear methods[17][18] were designed for nonlinear but stationary and deterministic systems. As a matter of fact, either natural or man-made systems are most likely to be both nonlinear and nonstationary. Conventional linear approaches fail to disclose such nonlinear, nonstationary properties. The universally accepted mathematical paradigm of data expansion in terms of an a priori established basis (for example, Fourier analysis) would need to be modified. A necessary condition to represent nonlinear and nonstationary data is to have an adaptive basis. A recently developed method, the Hilbert–Huang transform (HHT), by Huang et al. (1996, 1998, 1999) provides a

feasible way of analyzing the time-series data generated by a nonlinear and nonstationary system.

The HHT consists of two parts: empirical mode decomposition (EMD) and Hilbert spectral analysis (HSA). This method offers the same function of time-frequency representations (spectrograms) as what accomplished by wavelet transform (WT) or Wigner distribution (WD). Nevertheless, it does not require an a priori functional basis that may not fit most of the nonlinear, nonstationary data series. Accordingly, the results obtained by HHT reveal much sharper effect than those analyzed by the traditional time-frequency representation methods. Additionally, the HHT has demonstrated its capability of characterizing the physical meanings of empirical data acquired in a large variety of areas, including biomedical applications, ocean engineering, seismic studies, chemistry, chemical engineering, financial applications, image processing, etc. The extraordinary robustness of the method is its entirely empirical way of implementation. Table 2.2 summarizes comparisons among STFT (Short-time Fourier Transform), wavelet, and HHT analysis [19].

Table 2.2 Comparison among STFT, wavelet, and HHT analysis [19].

	STFT (Fourier based)	wavelet	HHT
Basis	A priori	A priori	A posteriori, Adaptive
Frequency	Integral transform over global domain, Uncertainty	Integral transform over global domain, Uncertainty	Differentiation over local domain, Certainty
Presentation	Energy in frequency space	Energy in time-frequency space	Energy in time-frequency space
Nonlinearity	No	No	Yes
Nonstationarity	No	Yes	Yes
Feature Extraction	No	Discrete: No Continuous: Yes	Yes
Theoretical base	Complete mathematical theory	Complete mathematical theory	Empirical



2.2.2 Empirical Mode Decomposition (EMD) method

EMD method was developed from the simple assumption that a signal could be considered as the composition of different simple, intrinsic modes of oscillations. Each linear or non-linear mode has the same number of extrema and zero-crossings. There is only one extremum between successive zero-crossings. Each mode should be independent of the others. In this way, each signal could be decomposed into a number of IMFs (intrinsic mode functions). The IMFs must satisfy the following criteria [20].

- (I) In the whole data set, the number of extrema and the number of zero-crossings must either equal or differ at most by one.
- (II) At any point, the mean value of the envelope defined by local maxima and the envelope defined by the local minima is zero.

An IMF represents a simple oscillatory mode compared with the simple harmonic function. With the definition, any discrete-time signal $x[n]$ can be decomposed as follows [20]:

- (1) Identify all the local maxima, and connect all the local maxima by cubic-spline interpolation to form the upper envelope.
- (2) Identify all the local minima, and connect all the local minima by cubic-spline interpolation to form the lower envelope. The upper and lower envelopes should enclose all the data points.

- (3) The midline of upper and lower envelope is designated as $m_1[n]$; and the difference between the signal $x[n]$ and $m_1[n]$ is the first component, $h_1[n]$; i.e.

$$x[n] - m_1[n] = h_1[n]. \quad (2.1)$$

Ideally, if $h_1[n]$ is an IMF, then $h_1[n]$ is the first component of $x[n]$.

- (4) If $h_1[n]$ is not an IMF, $h_1[n]$ is treated as the original signal to repeat steps (1)-(3) to obtain the new midline $m_{11}[n]$. Then, we obtain a new difference component

$$h_1[n] - m_{11}[n] = h_{11}[n]. \quad (2.2)$$

Such iterative sifting scheme is conducted till an IMF is obtained. Assume an IMF, $h_{1k}[n]$, is resulted in the k^{th} iteration, then

$$h_{1(k-1)}[n] - m_{1k}[n] = h_{1k}[n]. \quad (2.3)$$

We assign

$$c_1 = h_{1k}, \quad (2.4)$$

For the first IMF component obtained from the original data. Note that $c_1[n]$ should contain the finest scale or the shortest period component of the signal. The above four steps are called the “IMF construction” procedure.

- (5) To find the succeeding IMF components $c_i[n]$, $i \geq 2$, the first residual signal $r_i[n]$, $i=1$ is first obtained by subtracting $c_1[n]$ from $x[n]$:

$$r_1[n] = x[n] - c_1[n]. \quad (2.5)$$

Accordingly, the second IMF component $c_2[n]$ is obtained by replacing $x[n]$ by the residual signal $r_1[n]$ and then executing the IMF construction procedure. After repeating L times the entire process described in (1)-(5), we may obtain a set of L IMFs using $r_i[n]$ as the initialization for the i^{th} iteration.

$$\begin{aligned}
r_2[n] &= r_1[n] - c_2[n] \\
&\vdots \\
r_L[n] &= r_{L-1}[n] - c_L[n]
\end{aligned} \tag{2.6}$$

The decomposition process terminates when $r_L[n]$ becomes a monotonic function from which no more IMF can be extracted. By summing up Eqs. (2.5) and (2.6), we finally obtain

$$x[n] = \sum_{j=1}^L c_j[n] + r_L[n]. \tag{2.7}$$

As a consequence, signal $x[n]$ can be decomposed into L IMFs (empirical oscillatory modes) and a final residue $r_L[n]$, which can be considered as the baseline drift of $x[n]$. The IMFs, $c_1[n]$, $c_2[n]$, ..., and $c_L[n]$, individually consist of different frequencies ranging from the high to low frequency bands. The final residue $r_L[n]$ represents the central tendency of signal $x[n]$.

Block diagram in Fig. 2.5 illustrates the strategy of EMD method. To better understand the mechanism of EMD, we apply it to an ideal periodic signal simulated by sinusoidal functions with three different frequencies:

$$x[n] = 3 \cos(2\pi * 0.01 * n) + 2 \sin(2\pi * 0.005 * n) + \cos(2\pi * 0.003 * n) \tag{2.8}$$

Fig. 2.6 displays the simulated time sequence $x[n]$. The sampling frequency is 1,000 Hz. Four IMF components derived by EMD algorithm are shown in Fig. 2.7. As expected, the first components $c_1[n]$ contains 10 cycles; the second components $c_2[n]$ contains 5 cycles; the third components $c_3[n]$ contains 3 cycles with smaller amplitude; while the last components $c_4[n]$ nearly approximates DC with negligible energy. In this case, EMD succeeds in extracting the intrinsic rhythmic activities.

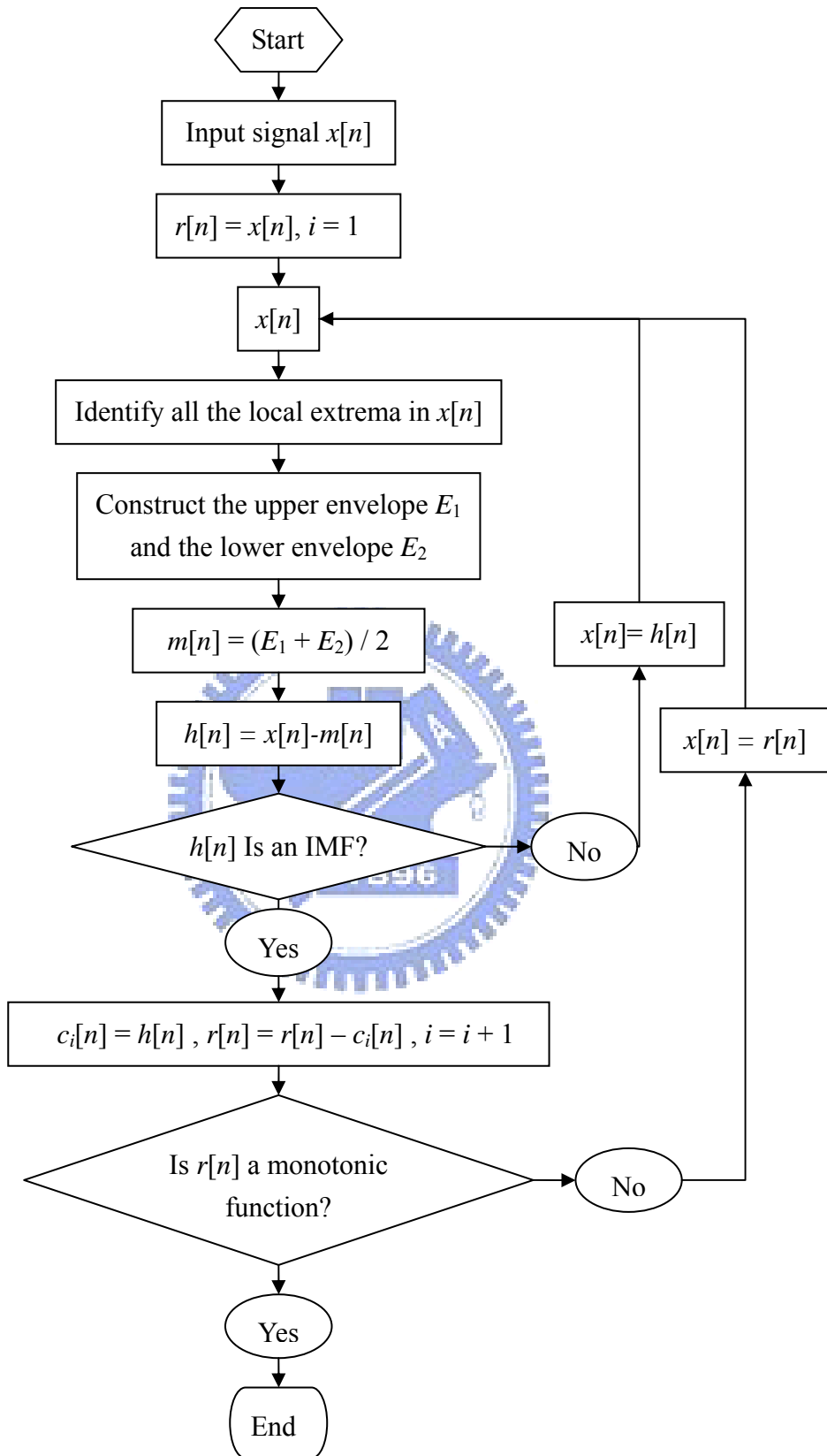


Fig 2. 5 Flow chart for EMD

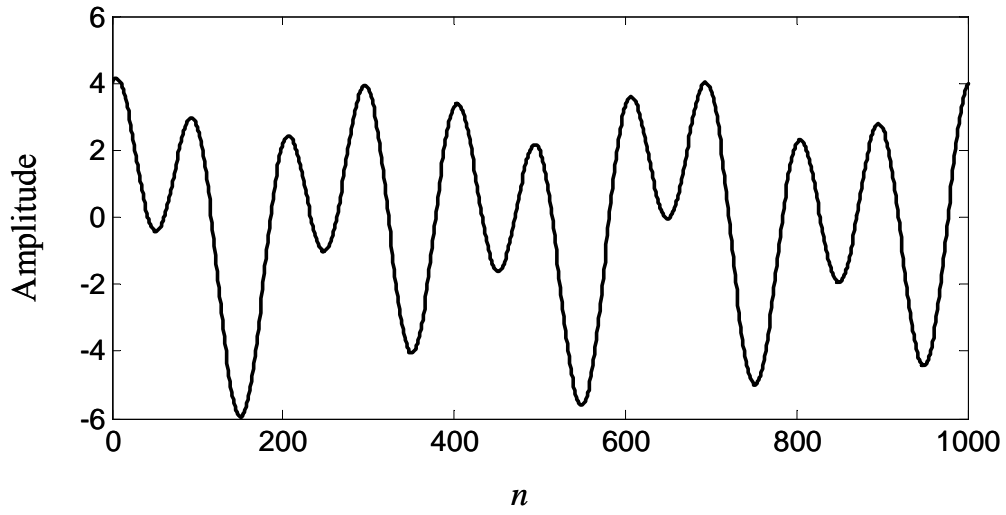


Fig 2. 6 An ideal time series $x[n]$ simulated by three sinusoidal components.

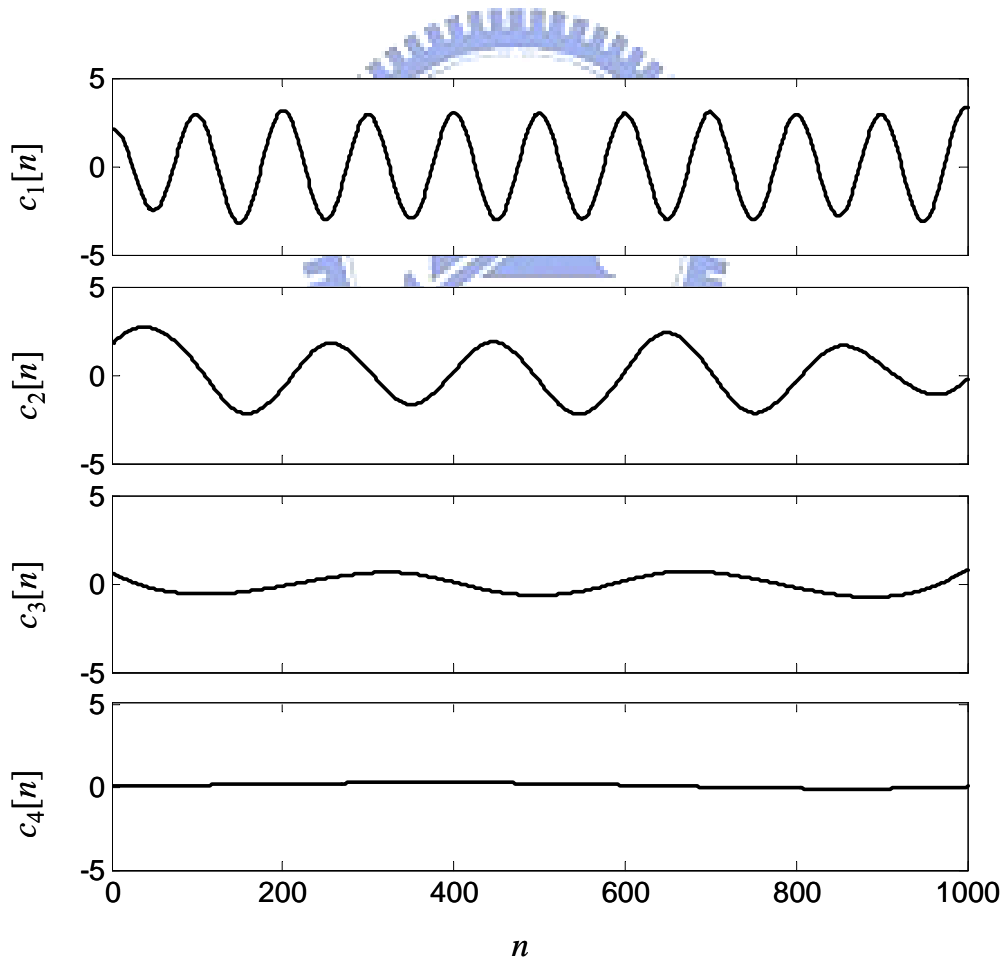


Fig 2. 7 First four IMF components of $x[n]$.

2.2.3 Discrete Hilbert transform (DHT)

The continuous Hilbert transform $\mathcal{F}[g(t)]$ of a continuous function $g(t)$ is described in Appendix C. Computerized implementation requires the discrete form for the transformation. DHT (discrete Hilbert transform) of a band-limited function $g[n]$ has the similar formula as the conventional HT, that can be considered as the convolution:

$$\mathcal{F}[g[n]] = g[n] * \lambda[n] \quad (2.9)$$

where

$$\lambda[n] = \begin{cases} 0, & n: \text{even} \\ \frac{2}{\pi}, & n: \text{odd} \end{cases} \quad (2.10)$$

The analytic signal, $z[n]$, of the real discrete time signal $g[n]$ is given by:

$$z[n] = g[n] + j\hat{g}[n] = a[n] \cdot e^{j\phi[n]} \quad (2.11)$$

Where $\hat{g}[n]$ is the discrete Hilbert transform of $g[n]$. The amplitude $a[n]$ and instantaneous phase $\phi[n]$ defined by:

$$a[n] = \sqrt{g^2[n] + \hat{g}^2[n]} \quad (2.12)$$

$$\phi[n] = \tan^{-1}\left(\frac{\hat{g}[n]}{g[n]}\right) \quad (2.13)$$

Then, the instantaneous phase are ready to be estimated based on Eqs. (2.13)

2.3 Analysis of Cardiorespiratory Phase Synchronization

The method presented here was originally developed for the analysis of two weakly coupled chaotic systems [21][22]. In this study, we made an assumption that each oscillator could be completely described by its output amplitude and output phase as a function of time[23]. The phase function accordingly can be reasonably defined for a time series with oscillatory rhythms in a relatively narrow frequency band.

Analytical representation of a real signal enables the illustration and formation of time-varying phase function. With the definition of the Hilbert transform $\hat{g}[n]$ for the time series $g[n]$, the time-varying phase $\phi[n]$ of $g[n]$ can be obtained by Eq.(2.12). Now let us consider the heart-rate time series $HR[n]$ and the respiratory time series $RP[n]$. The phase functions derived as above are denoted as $\phi_{HR}[n]$ and $\phi_{RP}[n]$, respectively. Next, the difference $\phi[n]$ between the phase functions above is

$$\phi[n] = \phi_{RP}[n] - \phi_{HR}[n]. \quad (2.14)$$

The heart-rate time series and the respiratory time series are synchronized if this phase difference is constant within a small tolerance. That is,

$$|\phi[n]| < \delta, \forall n \quad (2.15)$$

with δ being a constant offset. Note that the phase difference $\phi[n]$ needs not be approximately zero.

Unfortunately, noise and other sources of interference in both time series may lead to random-like “phase jumps” of $\pm 2\pi$ in both phase sequences $\phi_{HR}[n]$ and $\phi_{RP}[n]$. Thus, even in a synchronized state, the phase difference $\phi[n]$ may not be constant anymore. To resolve this issue, a straightforward way is to apply modulo- 2π operation to $\phi[n]$ as below

$$\psi[n] = \phi[n] \bmod 2\pi \quad (2.16)$$

that assumes a more generalized criterion for phase synchronization given in (2.15), that is, $\phi[n] \pm 2n\pi$ (n : any integer) is bounded by a constant tolerance. Finally, an unbiased indicator to quantify the degree of phase synchronization between two systems can be designed as follows

$$\gamma = \langle \cos \psi[n] \rangle^2 + \langle \sin \psi[n] \rangle^2 \quad 0 \leq \gamma \leq 1, \quad (2.17)$$

where brackets $\langle \dots \rangle$ denote the average over a specified interval N samples [24][25].

The indicator γ is called “degree of phase synchronization.” As a consequence, γ offers an unambiguous measurement for the stationarity of $\psi[n]$. Time-varying behavior of γ 's provides a quantitative interpretation of phase-synchronization scenario for cardiorespiratory interaction.

Theoretically, a large value of γ , particularly when approaching 1, strongly infers that $\psi[n]$ is constant and therefore concludes that both time series are highly synchronized in a statistical sense. As a consequence, the segments of large $\psi[n]$ (above a threshold) are considered to be the time epochs of good cardiorespiratory phase synchronization. On the other hand, a small γ signifies the state of poor phase synchronization. Particularly, the exclusive case $\gamma=0$ indicates the complete phase

desynchronization between heart-beat and respiratory sequences because the values of $\psi[n]$ are equally distributed in the range $[-\pi, \pi]$.

However, due to artifacts or other factors, empirical data may always contain some falsely synchronized patterns although the systems are completely desynchronized. Thus, the lower bound of meaningful γ was estimated with the help of so-called surrogate data, that is, artificial data without any coupling which were constructed on the basis of the original data. This process yielded $\gamma = 0.14$ as an estimation of the lower bound, that is, any value $\gamma \leq 0.14$ would be considered as completely desynchronized[26][27].

Fig 2.8 presents an example to illustrate the scheme of cardiorespiratory phase synchronization analysis. Figs 2.8(a), (c), and (e) demonstrate the unsynchronized example; while Figs 2.8(b), (d), and (f) present the case of good synchronization. In Figs 2.8(a) and (b), original respiratory signal (thick curves) and constructed HR (heart rate) sequences (thin curves) appear to de-harmonize in Fig 2.8(a); whereas they oscillate in a well synchronous tempo in Fig 2.8(b) with waveform patterns approximating sinusoid. As a result, magnitude of phase difference in Fig 2.8(c) increases with time, revealing typical phase-difference trait for unsynchronized case. On the other hand, a nearly zero and constant phase difference characterizes the perfect synchronized cardiorespiratory-interaction behaviors. Histogram illustration for γ distributing with regards to phase difference ψ exhibits a wide-range distribution with small magnitude for unsynchronized case (Fig 2.8(e)). Nevertheless, values of γ for synchronous activity normally concentrate in a narrow range of ψ with significantly large magnitude (Fig 2.8(f)).

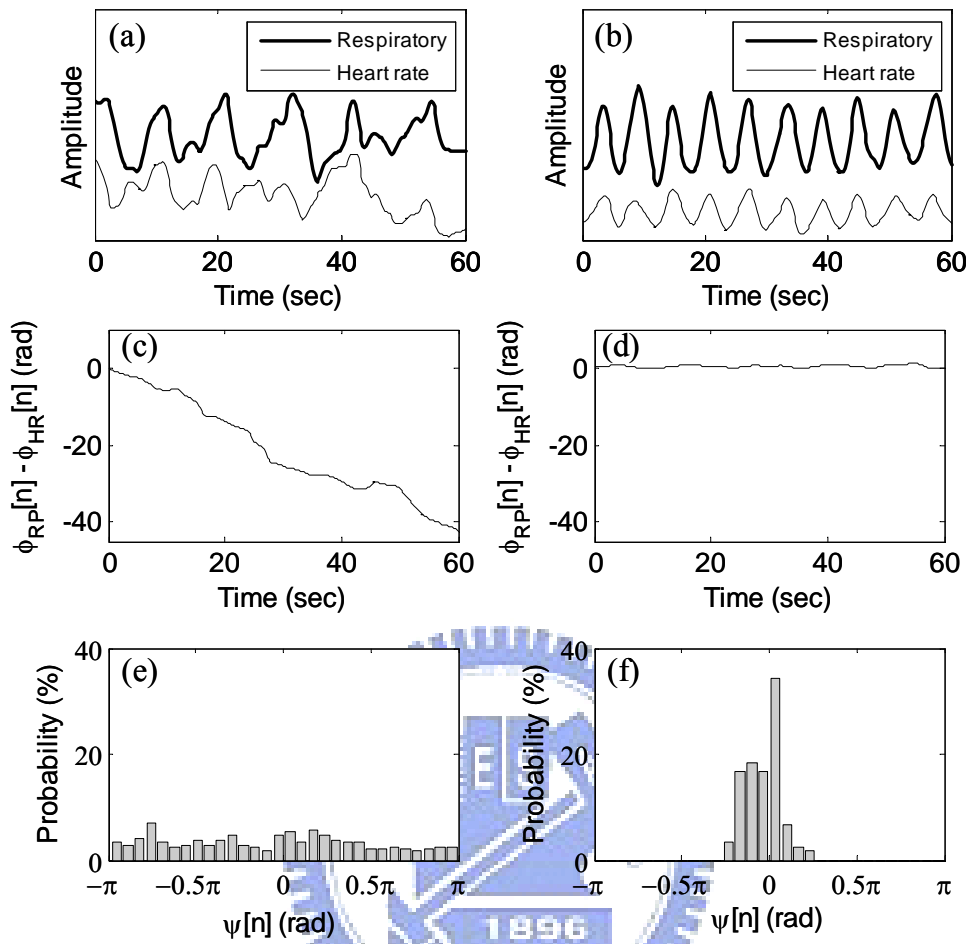


Fig 2.8 Examples for cardiorespiratory desynchronization (left column) and synchronization (right column).

Chapter 3

Experiment and Signal Analysis

Chapter 3 contains two major sections. Section 3.1 presents the practical setup, protocol, and physiological signal acquisition employed in this study. Section 3.2 describes the technical strategies for investigating the cardiorespiratory phase synchronization.

3.1 Experimental Setup and Procedure

This study involved two groups of subjects, the experimental group including subjects with Zen-meditation experience and the control group including subjects without any meditation experience. Background of subjects in each group is listed in

Table 3.1 Subjects of experimental and control groups

	Experimental group	Control group
Number of subjects	6	6
Sex (male : female)	3:3	5 : 1
Age (years)	27.6 ± 2.3	26 ± 1.1
Meditation experience (years)	6 ± 1.9	

3.1.1 Control Group

In the experiment, we collected 30-min ECG and respiration signals for each subject. In the control group, each recording involved four sessions in which the subject was asked to breathe at different rates. In the first 5-minute session, the subject breathed naturally at their normal breathing rate. In the following two sessions of 10-minute duration each, the subject was asked to follow an auditory-cue guidance to breathe at the rate of respectively 10 and 6 breaths per minute. Finally, the subject breathed again at the normal rate in the fourth 5-minute session. Fig.3.1 illustrates the experimental procedure.

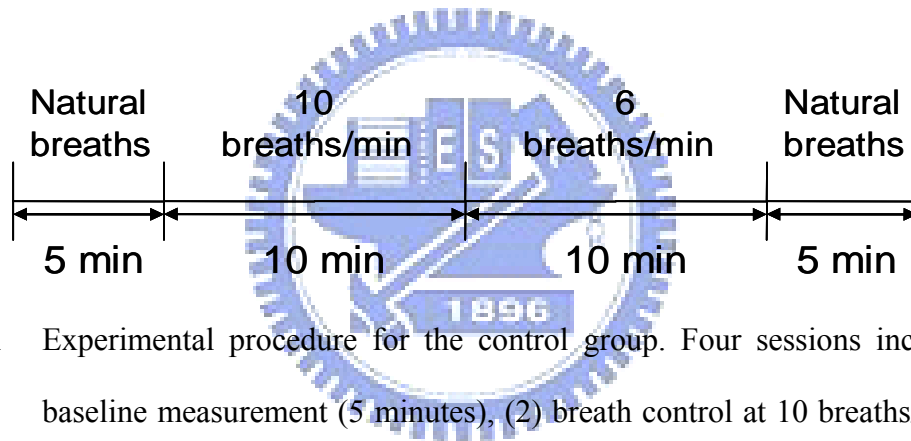


Fig 3.1 Experimental procedure for the control group. Four sessions include (1) baseline measurement (5 minutes), (2) breath control at 10 breaths/min (10 minutes), (3) breath control at 6 breaths/min (10 minutes), and (4) post-test natural breathing (5 minutes).

3.1.2 Experimental Group

ECG and respiration signals of experimental subjects (Chan-meditation practitioners) were collected while they practiced Chan meditation in the meditation course held in a formal meditation center. Subjects were not required to follow any protocol, instead, they only took part in their routine practice in the 90-minute class as usual. Appendix B briefly describes the procedure of the practice.

After the Chan-meditation class, subjects were interviewed immediately. The oral report of their meditation scenario was recorded.

3.1.3 Signal Acquisition

Fig.3.2 demonstrates the recording system for collecting the physiological signals employed in the control group. The signals recorded from a subject are amplified, pre-filtered and digitized by g.BSamp biosignal amplifier manufactured by Cortech Solutions. The digital signals are transmitted to a desktop through USB interface and then recorded with the built-in data-acquisition software (Chart4). The ECG and respiratory signals were recorded by the system simultaneously and digitized with a sampling frequency of 1,000 Hz.

The ECG and respiration signals were recorded simultaneously at 1000 Hz sampling rate using PowerLab/16SP recording system (ADInstruments, Sydney, Australia; see Fig. 3.2). Furthermore, the ECG signal was pre-filtered by a 0.3-200 Hz bandpass filter, and the respiratory signal was pre-filtered by a lowpass filter with cutoff frequency of 5 Hz. A 60-Hz notch filter was applied to remove artifacts from power line or the surroundings.

For experimental group, the electrocardiogram (ECG) and respiration signals were recorded simultaneously at 512Hz and 128Hz using NuXus-4 recording system (TMS International BV, Oldenzaal, The Netherlands; see Fig.3.3). The respiratory signals was recorded using a piezo-electric transducer (NX-RSP1A, TMS International BV, Oldenzaal, the Natherlands) wrapped around the belly passing the navel.

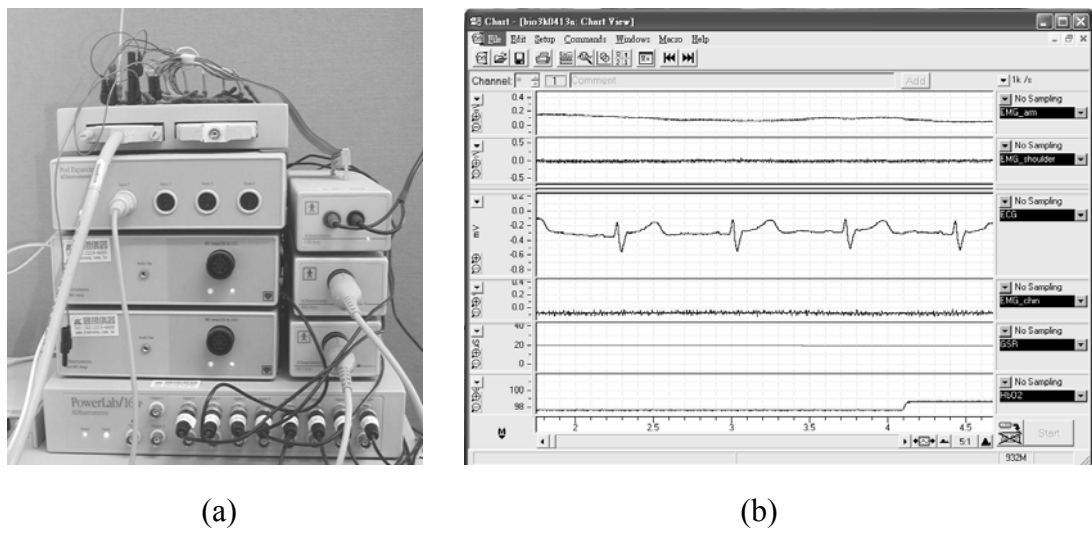


Fig 3.2 Physiological signal recording system for control group: (a) Bio-amplifiers, and (b) digitization and on-line monitoring system.

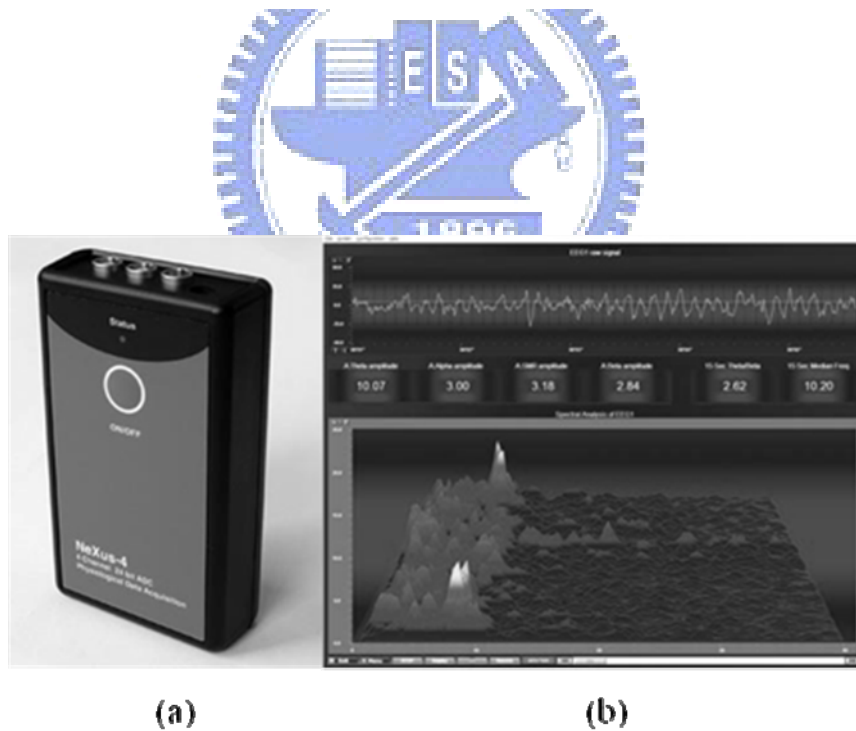


Fig 3.3 Physiological signal recording system for experimental group: (a) Bluetooth Bio-amplifiers, and (b) digitization and on-line monitoring system.

3.1.4 Measurement of ECG signal

The recording electrodes (Medi-Trace 200 Foam Electrode) are manufactured by Kendall-LTP, as shown in Fig. 3.4 (a). In this study, the ECG recording applied the bipolar limb-lead I electrode placement in control group and applied the bipolar limb-lead II electrode placement in experimental group. By convention, limb-lead I has the positive electrode on the left arm, and the negative electrode on the right arm, with an electrode on the right leg serving as a reference electrode. Such kind of bipolar configuration accordingly measures the potential difference between two arms. For convenience of applying electrodes to voluntary subjects, we adjusted the placement by attaching the positive/negative electrode to the left/right inner wrist, with the reference electrode placed on the right ankle (Fig 3.4).

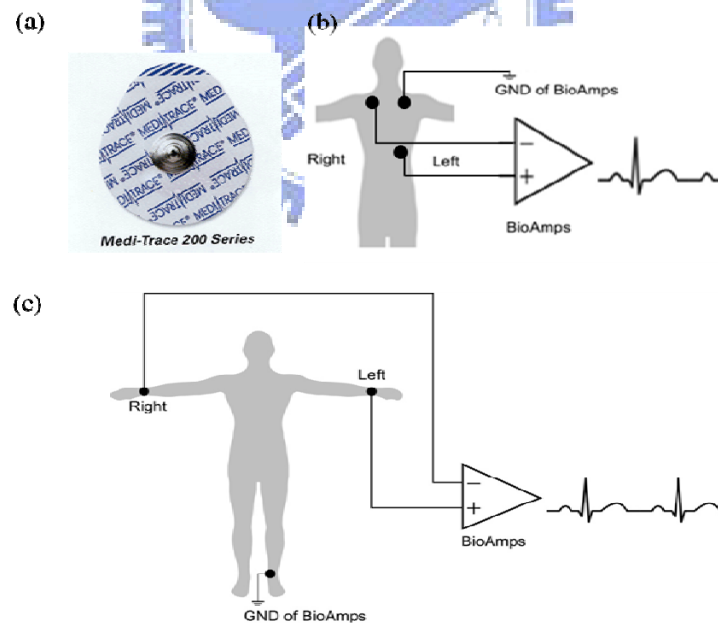


Fig 3.4 (a) ECG electrode, (b) Bipolar limb-lead II electrode placement(experimental group) and (c) Bipolar limb-lead I electrode placement(control group).

3.1.5 Measurement of respiratory signal

The behavior of respiration accompanying the chest/abdominal movement is recorded by the piezo-electric transducer (Model 1132 Pneumotrace II (R)) made by UFI, as shown in Fig. 3.5. The electrical conductivity increases linearly with the chest/abdominal circumference associated with respiration, and the sine-wave like signal can be recorded. Fig 3.6 demonstrates the waveform pattern during inspiration and expiration.



Fig 3. 5 Piezo-electric respiratory transducer

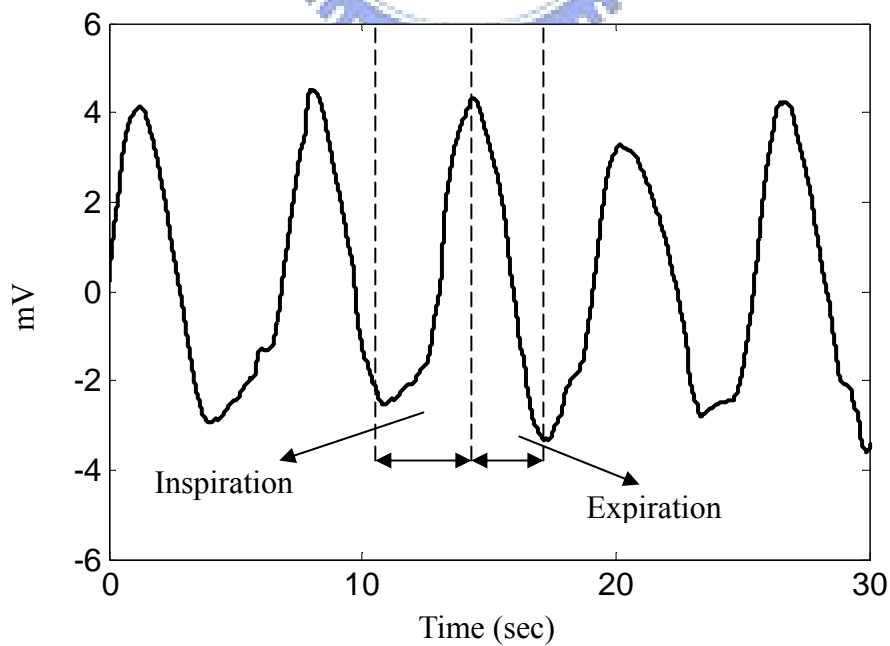


Fig 3. 6 Respiratory signal

3.2 Cardiorespiratory Phase Synchronization Analysis

The strategy for analyzing the cardiorespiratory phase synchronization is illustrated in the flow chart in Fig 3.7.

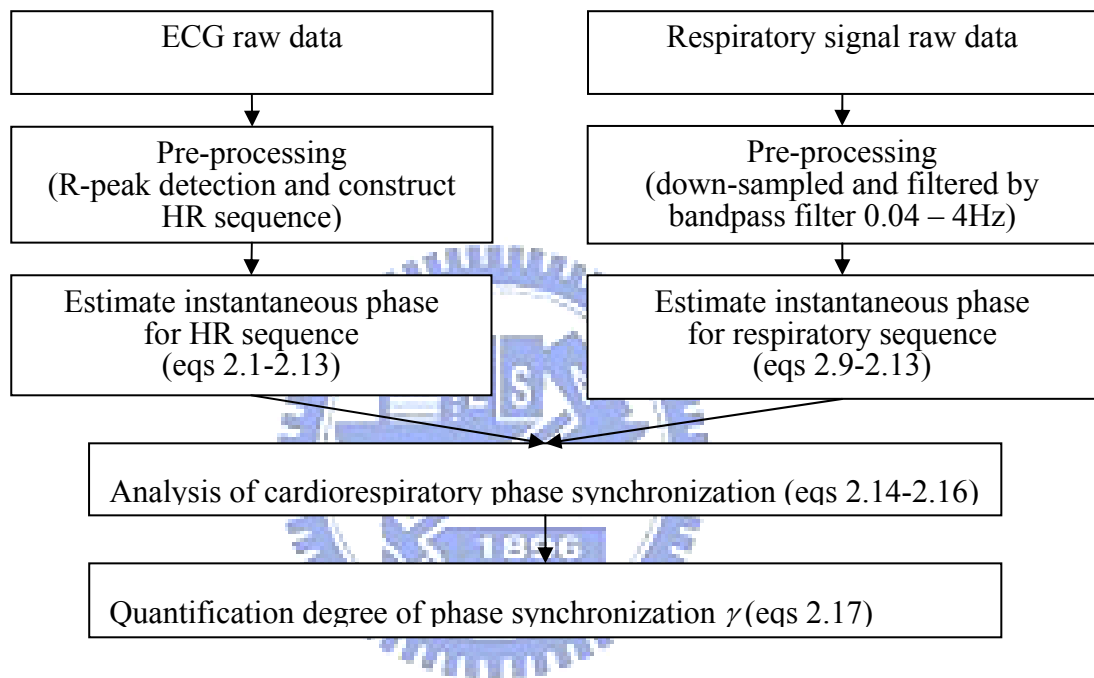


Fig 3.7 Flow chart for the strategy for analyzing the cardiorespiratory phase synchronization.

Step 1: Pre-processing

In the HR pre-processing step, R-peak detection algorithm (Appendix A) was first applied to ECG signal to extract all R peaks in the ECG and then construct the RRI (R-to-R interval) time series. RRI sequence represents a series of sample data (events) digitized at the occurrence of R peaks. Since empirical signals are mostly pseudo-periodic (that is, a typical prototype repeats at a varying pace), the RRI

sequence accordingly corresponds to a digital signal sampled with non-uniform sampling rate. In the phase synchronization study, sampling rate is required to be constant not only for a time series at different times but for both sequences under assessment. To uniform the sampling rate, we firstly interpolated the RRI sequences by Cubic Spline and then re-sampled the interpolated signal with an equivalent sampling rate of 4Hz. Finally, the reciprocal of sampled data was computed as the heart-rate value $HR[n]$.

In the RP (respiratory) pre-processing step, the original respiratory signal was firstly down-sampled into a time series with the sample rate of 4Hz. To obtain the respiratory time series $RP[n]$, a bandpass filter with passband 0.04-0.4Hz was applied to reduce the baseline drift and high-frequency noise and therefore facilitate the instantaneous phase analysis.

Step 2: Estimation of instantaneous phase for HR and RP sequences

The strategy for estimating the instantaneous phase for both HR and RP sequences is described in Fig 3.8. EMD algorithm (Fig 2.5) was applied to heart-rate sequence $HR[n]$ to obtain the decomposed components (IMF_{*i*}) $c_i[n]$. Fig 3.9 displays the first four IMF components for a control subject (identified as #5). Note that the first component has the highest frequency and the succeeding decomposed components have frequencies decreasing at the rate of IMF1 (0.07~0.4Hz) 、IMF2 (0.03~0.07Hz) 、IMF3 (0.01~0.03) 、IMF4 (0.005~0.01)

It has been reported that the highest-frequency component of HR sequence reflected the influence of respiration. We hence investigated the cardiorespiratory phase behavior based on the decomposed IMF_1 of HR sequence [28]. DHT was then applied to IMF_1 of HR sequence ($c_1[n]$) and the pre-processed RP sequence ($RP[n]$). In this study, DHT was implemented through MatLab built-in function. Now we were ready to estimate the instantaneous phase functions $\phi_{HR}[n]$ and $\phi_{RP}[n]$ by applying equation (2.13) to the DHT results.

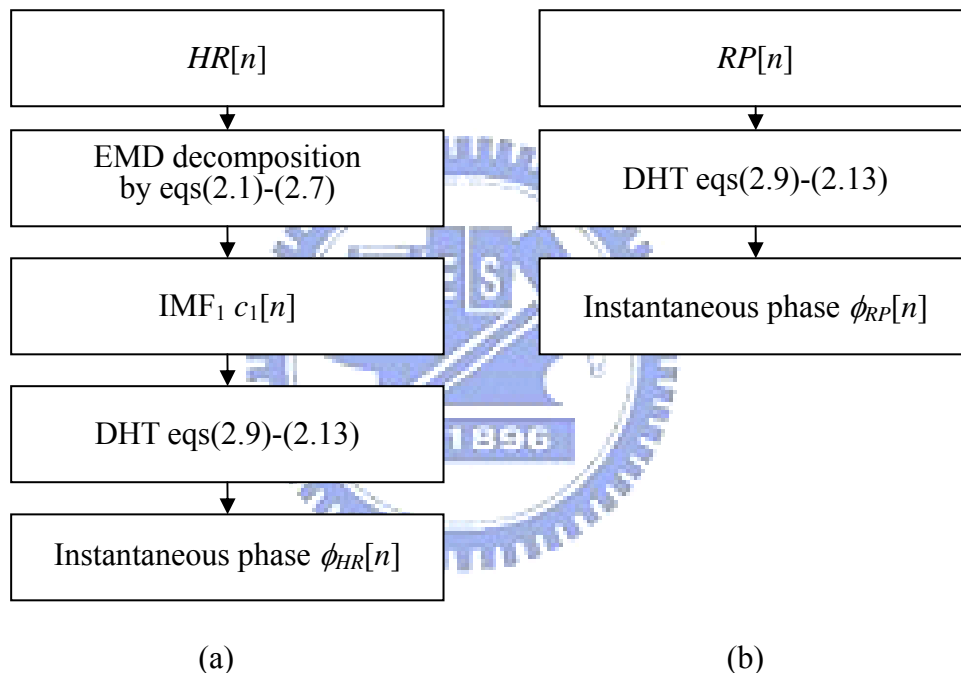


Fig 3. 8 Flow chart for the strategy for estimating the instantaneous phase of (a) HR and (b) RP sequences.

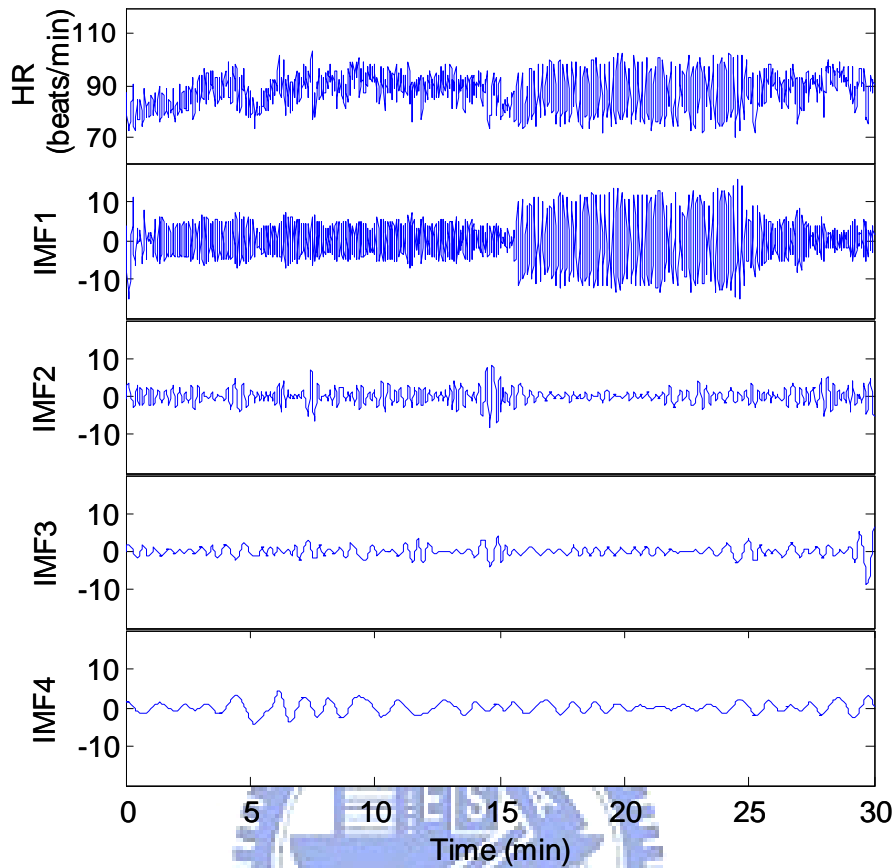


Fig 3. 9 The first four IMF components $c_i[n]$, $i=1-4$ of the HR time series for control subject #5.

Step 3: Analysis of cardiorespiratory phase synchronization

In this step, the phase difference between $\phi_{RP}[n]$ and $\phi_{HR}[n]$ was monitored by simply applying equation (2.14), $\varphi[n] = \phi_{RP}[n] - \phi_{HR}[n]$, which allowed us to scrutinize the time-varying phase synchronous scenario with eyeballs. As plotted in Fig 3.10 (result for experimental subject #3), good cardiorespiratory phase synchronization occurs during 0th-12th minute and 16th-20th minute epochs where the phase difference appears to be piecewise flat (constant). However, significant dips always emerge at the discontinuities of consecutive flat stairs.

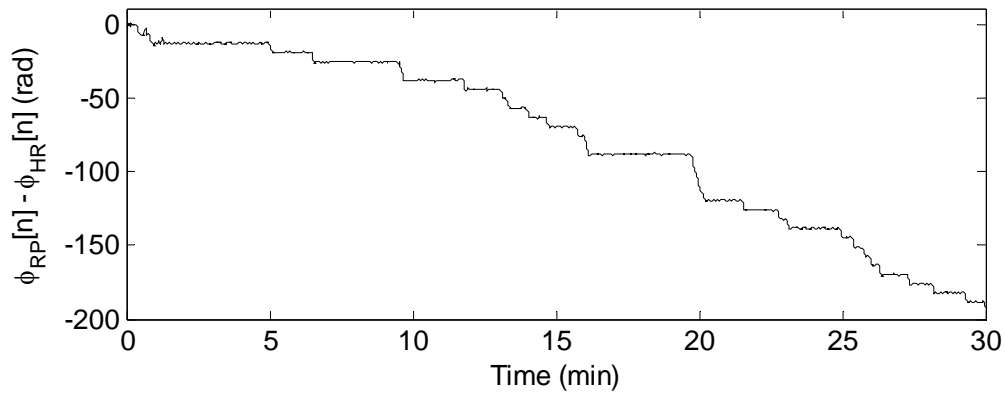


Fig 3. 10 The 30-minute cardiorespiratory phase difference scenario for experimental subject #3.

Step 4: Assessment of degree of phase synchronization γ

With a window size of one minute, degree of phase synchronization γ was evaluated every 10 seconds by a 10-sec moving step (or, overlapping by 50 seconds). The running-window scheme is illustrated in Fig 3.11. Time-dependent γ (Fig. 3.12) clearly reveals the evolution of cardiorespiratory interaction based on degree of phase synchronization. The result well coincides with Fig 3.10 in the sense that γ increases as ψ becomes constant.

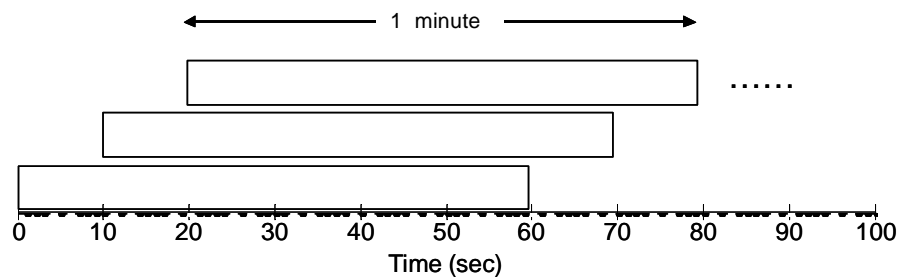


Fig 3. 11 Running-window scheme used to assess the temporal evolution of degree of cardiorespiratory phase synchronization.

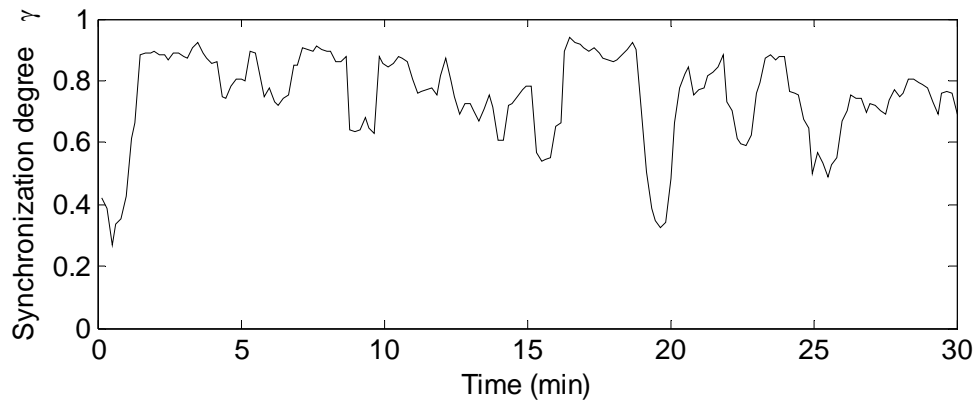


Fig 3. 12 Degree of phase synchronization γ (experimental subject #3) evaluated with the running-window scheme (size 1 minute, moving step 10 seconds).



3.3 Strategy for Estimating Respiratory Rate

Respiratory rate is one of the important control factors in this study. To construct the time-dependent respiratory sequence, we followed the same approach as that adopted for creating the HR sequence. The first step was to identify all maximal peaks in the original respiratory signal (Appendix A), from which we could derive the PPI (peak-to-peak interval) sequence. The raw PPI sequence has the issue of varying periods between adjacent samples, similar to the RRI sequence derived from ECG. Two steps were employed to reconstruct a sequence with uniform sampling rate: 1) Cubic Spline interpolation, and 2) re-sampling with a constant sampling rate of 4Hz. Then, the RpR (respiratory rate) sequence was obtained by taking reciprocal of each sample datum of the re-sampled PPI sequence. Fig 3.13 displays the smoothed RpR sequence (experimental subject #3) computed by moving-average filter using one-minute window size and 10-sec moving step.

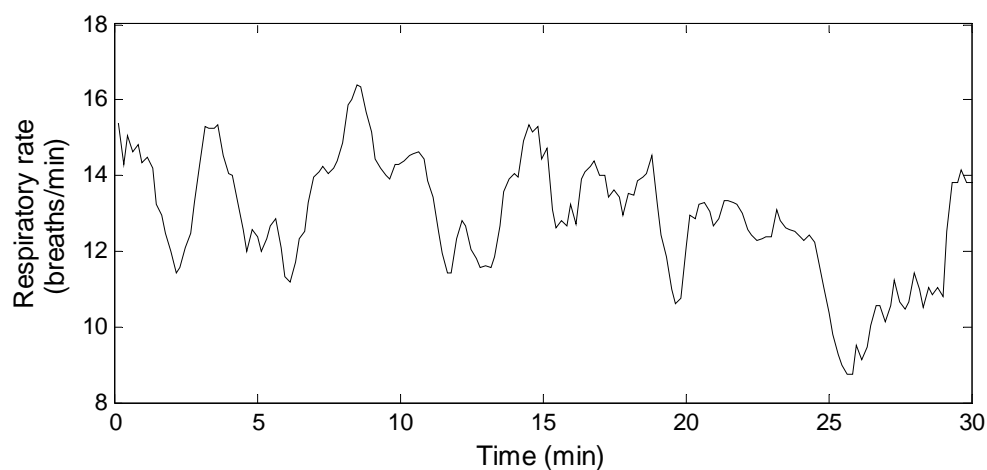


Fig 3. 13 Time-varying respiratory rate analyzed for experimental subject #3.

Chapter 4

Results and Inspection

This chapter presents the results of our study on cardiorespiratory phase synchronization. We particularly emphasize the comparison between experimental and control groups. Sections 4.1 and 4.2 report the results for controls and Chan-meditation practitioners, respectively. Finally, we draw a systematic comparison of the quantitative cardiorespiratory interactions between two groups in Section 4.3.

4.1 Results for control group

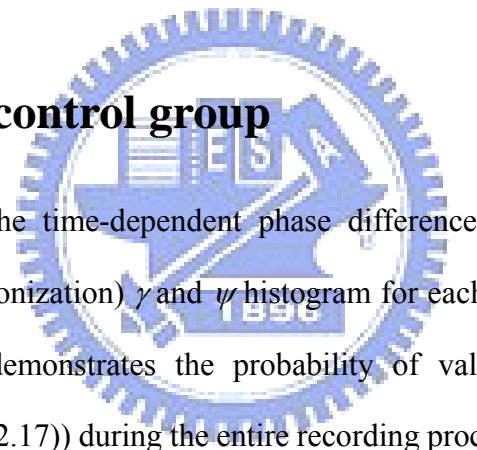
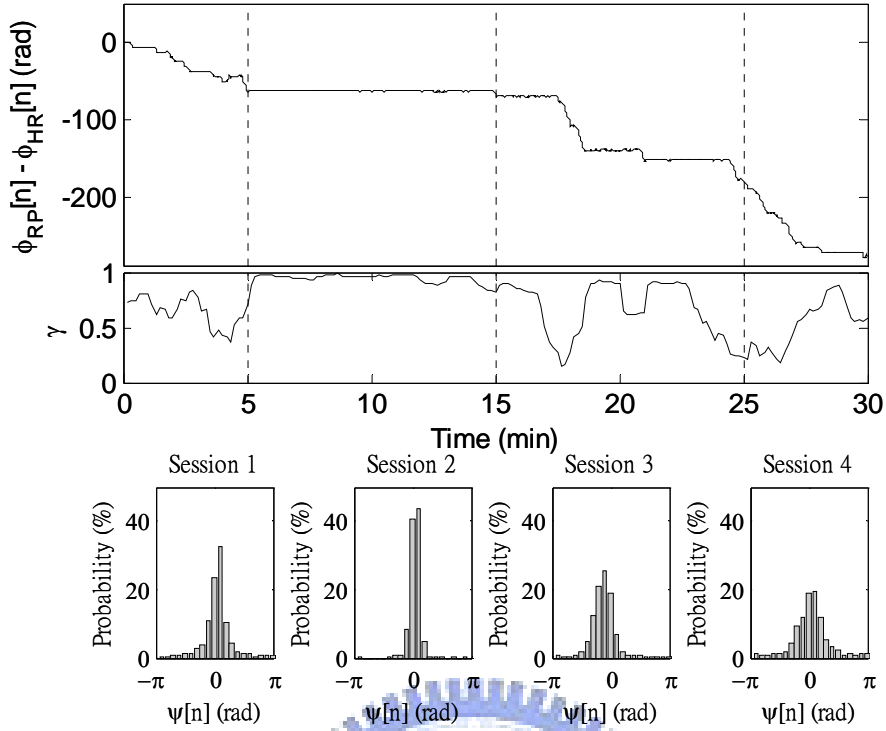
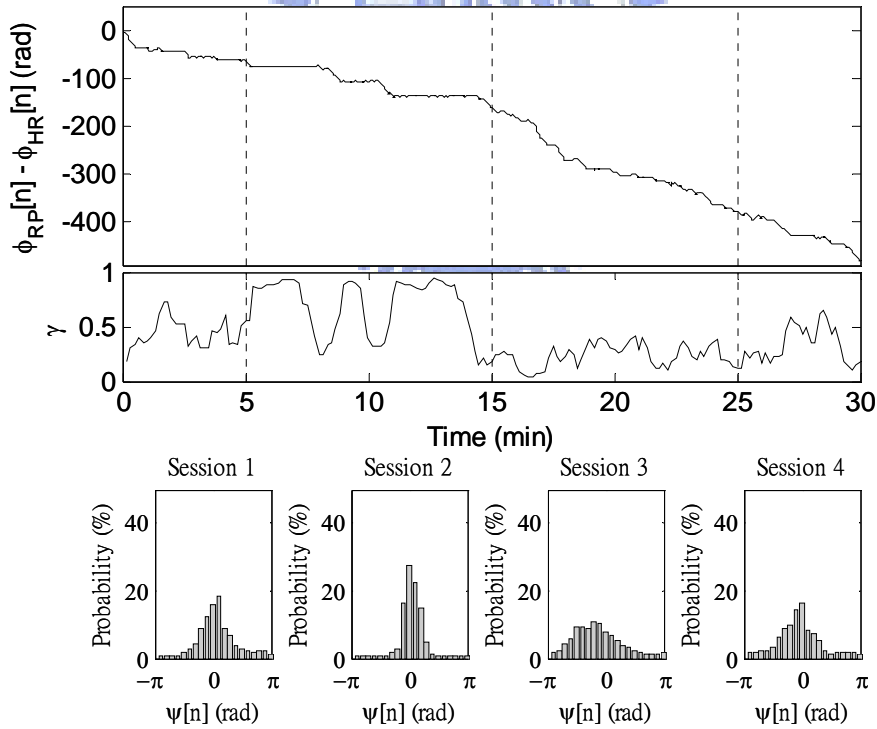


Fig 4.1 displays the time-dependent phase difference φ time-dependent dps (degree of phase synchronization) γ and ψ histogram for each individual control. The plot of ψ histogram demonstrates the probability of value of phase difference (evaluated by equation (2.17)) during the entire recording procedure. The phenomenon of leveling-out (constant) ψ in the 2nd session (breathing control at 10 breaths/min) is particularly evident for all subjects. As a result, dps γ becomes larger signifying the enhanced cardiorespiratory phase synchronization at this particular breathing rate. In addition, all six ψ histograms appear to be most focalized in this session. Such a focalized ψ histogram infers the phenomenon of constant ψ and, accordingly, higher degree of phase synchronization γ , in the second session.

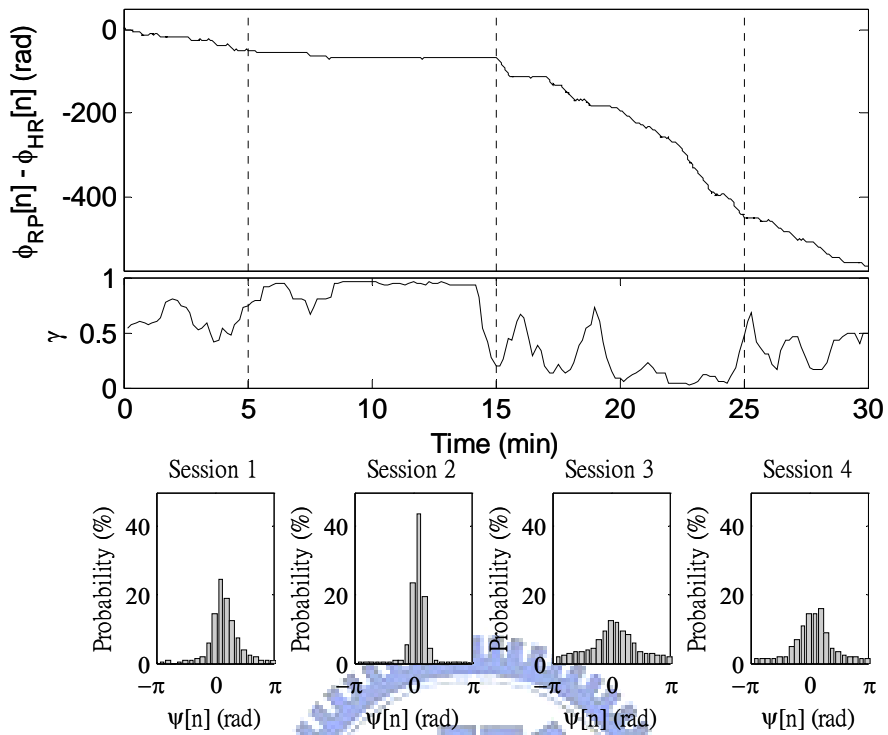


(a) control subject #1,

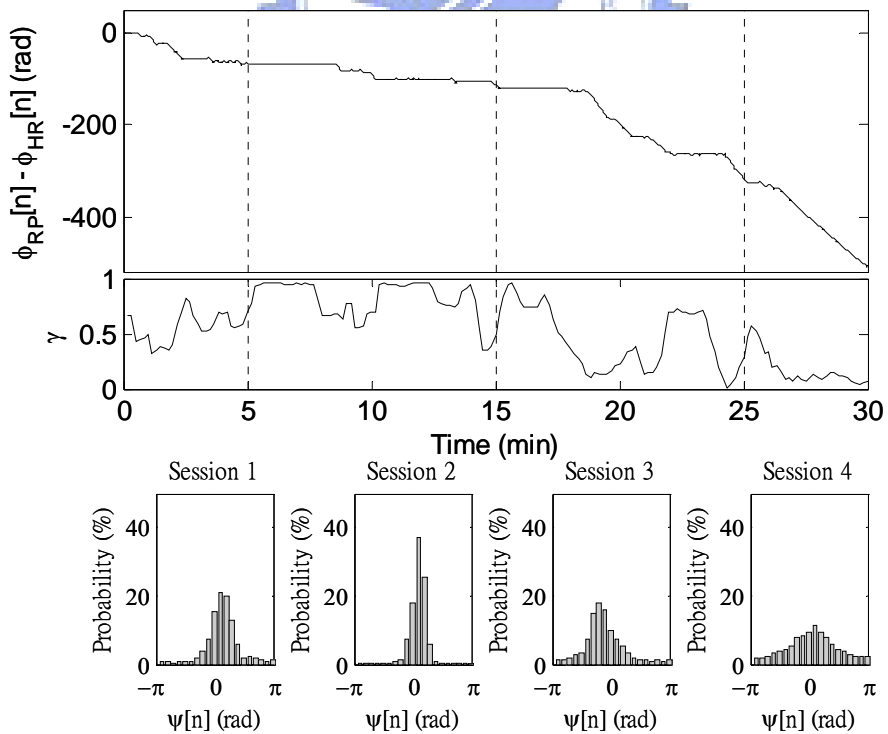


(b) control subject #2,

Fig 4.1 Analysis of cardiorespiratory phase synchronization for control group. (a)-(f) are the results for control subjects #1 to #6, respectively. Results include 1) time-dependent phase difference ψ , 2) time-dependent dps γ , and 3) ψ histogram.

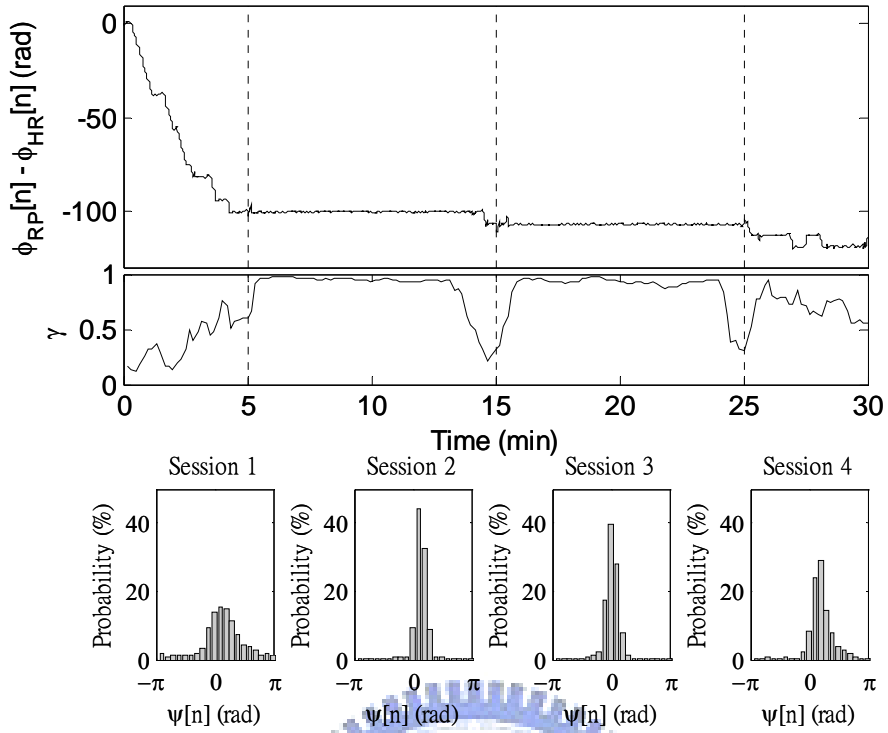


(c) control subject #3,

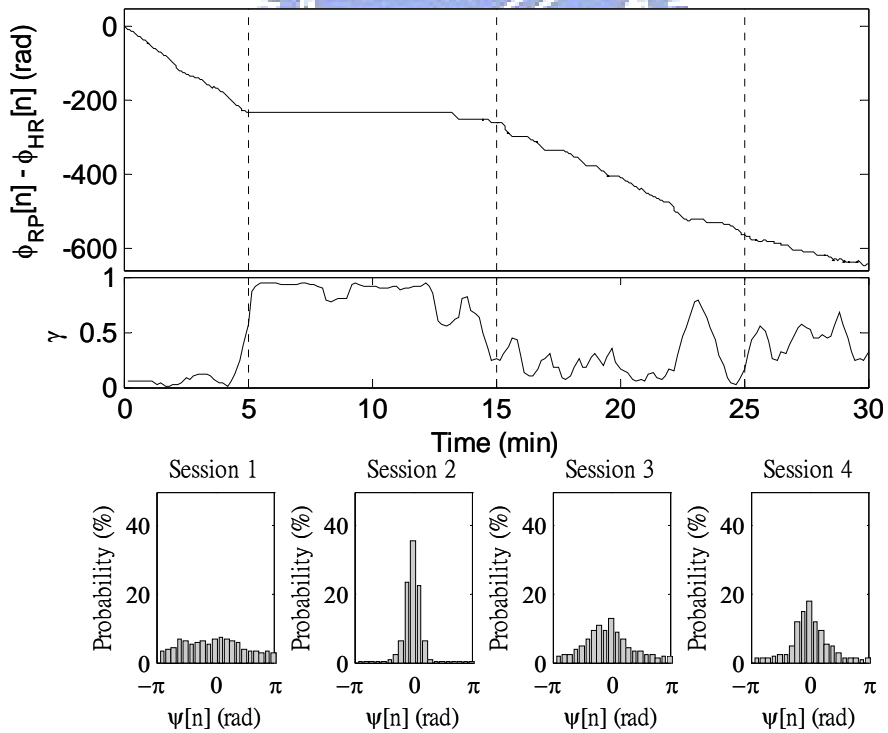


(d) control subject #4,

Fig 4.1 (continue).



(e) control subject #5,



(f) control subject #6,

Fig 4.1 (continue).

The gray-level monochrome image in Fig 4.2 illustrates the temporal evolution of γ for all the control subjects, with brighter gray corresponding to larger γ . All subjects exhibit consistently higher γ in the 2nd session, that is further confirmed by the highest average *dps* in Fig 4.3.

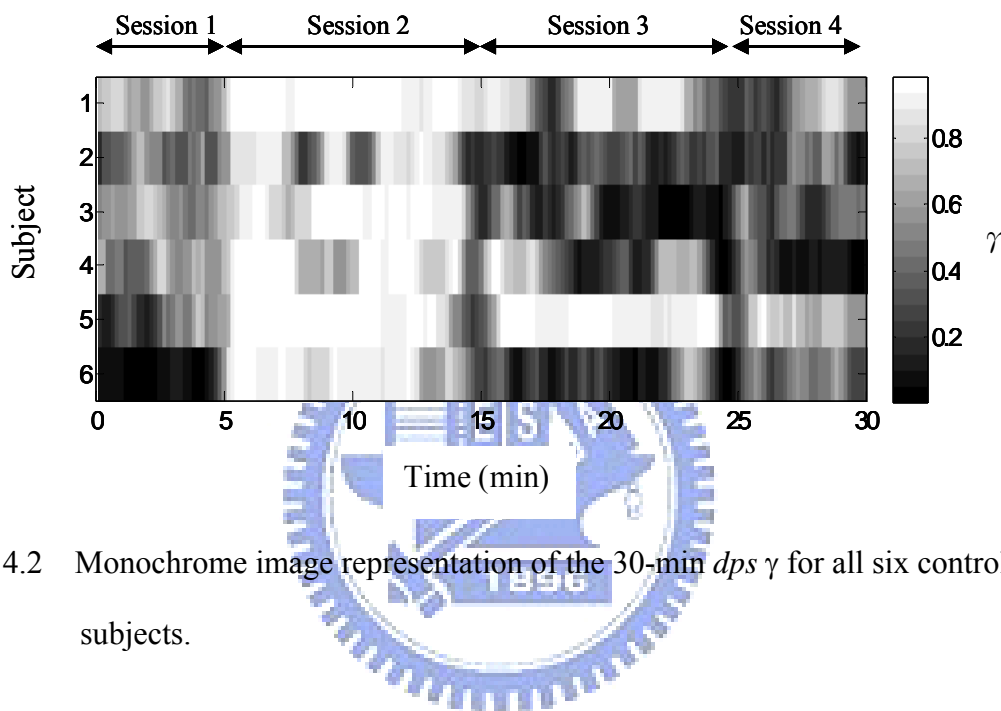


Fig 4.2 Monochrome image representation of the 30-min *dps* γ for all six control subjects.

On the contrary, breathing control at the rate of 6 breaths/min (in the 3rd session) resulted in a reduction of average *dps* in five subjects. One possible inference from the results is that normal subjects without meditation training are not used to such low respiratory rate. They might feel uneasy during the test in the 3rd session while making effort to tune in their breathing tempo to the computer generated audio cue. Consequently, they exhibited the poorer cardiorespiratory phase synchronization.

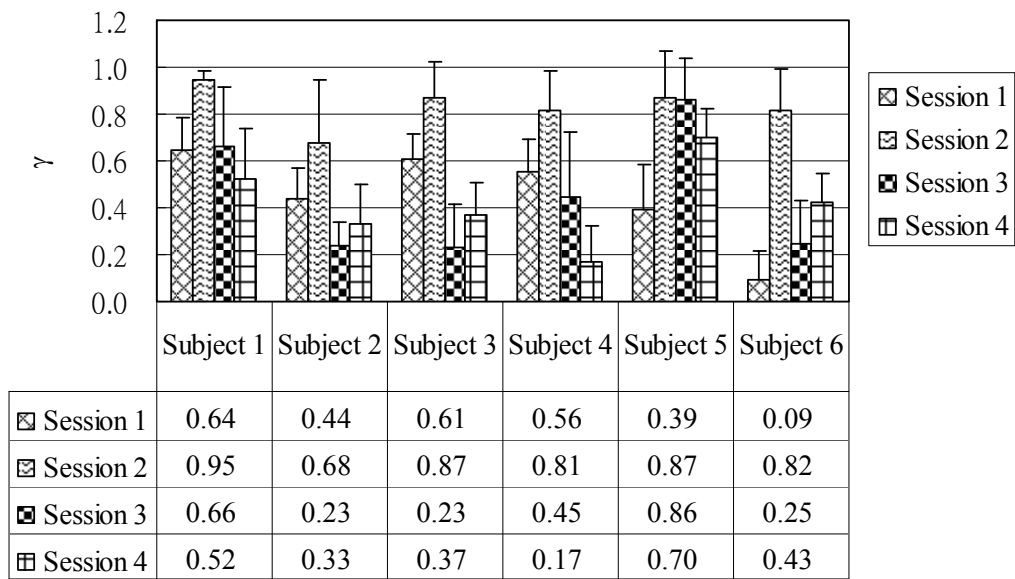


Fig 4.3 Average *dps* in each session for control subjects #1 to #6.

We applied t-test to justify the statistical significance of the distinction of average *dps* in different sessions. As shown in Fig 4.4, each bar corresponds to the average *dps* of all 6 control subjects in the same session, with the standard deviation depicted by a short line segment on the top. The symbol ** denotes significant difference ($p < 0.02$) justified by t-test existing between the second session and the other sessions, that is, the 2nd and 1st sessions, the 2nd and 3rd sessions, and the 2nd and 4th sessions.

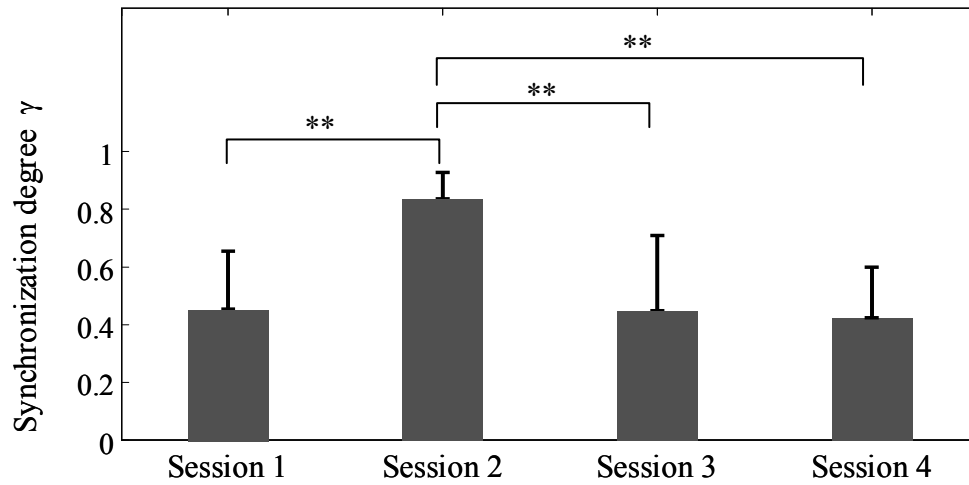


Fig 4.4 Average dps of all 6 control subjects in the same session. The symbol ** denotes significant difference ($p < 0.02$) justified by t-test existing between the second session and the other sessions.



4.2 Results for experimental group

In the study on experimental group, Chan-meditation practitioners were not requested to follow any experimental protocol during the physiological signal recording. In that case, they could freely meditate into the deep, transcendental consciousness, *Alaya* state, and even the realm of true-self halo wisdom. *Alaya* state is the so-called Eighth consciousness that is the seed consciousness of seven consciousnesses including eye, ear, nose, tongue, body, ideation (mind monkey), and obscuration (subliminal) consciousness. Alternatively speaking, these seven consciousnesses are founded on the *Alaya* consciousness. In Chan-meditation practice, the only essence of meditation is to transcend all the seven consciousnesses and *Alaya* consciousness to attain and eventually realize the true-self halo wisdom. Each practitioner thus has his/her own unique meditation scenario. In order to catch a rough outline of how the subject experienced in the entire meditation course, we conducted an interview with the experimental subject right after the recording.

As a consequence, time-dependent $dps \gamma$ illustrated in the form of monochrome image reveals different synchronization scenarios in Fig 4.5. Could temporal evolution of ψ or γ reflect various consciousness state of meditation? Further research work is required to explore the unknown realm of meditation consciousness.

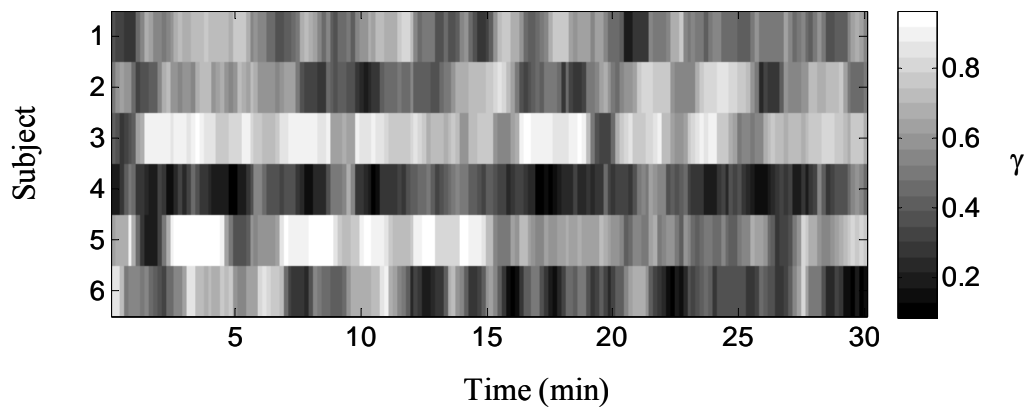


Fig 4.5 Monochrome image representation of the 30-min *dps* γ for all six experimental subjects

In this preliminary study, we intended to summarize the statistical trend of quantitative results as follows. Fig 4.6 displays the respiratory-rate (RR) histograms for each meditation practitioner during the entire Chan-meditation course. Normal respiratory rate for adults is about in the range of 16-20 breaths per minute. In comparison to the range, Chan-meditation practitioners in general had slower breathing (average respiratory rate: 12.18 breaths/min) during the meditation. Among these six practitioners, subject #6 particularly had a slowest breathing rate, mainly in the range of 5-10 breaths/min, during Chan-meditation course.

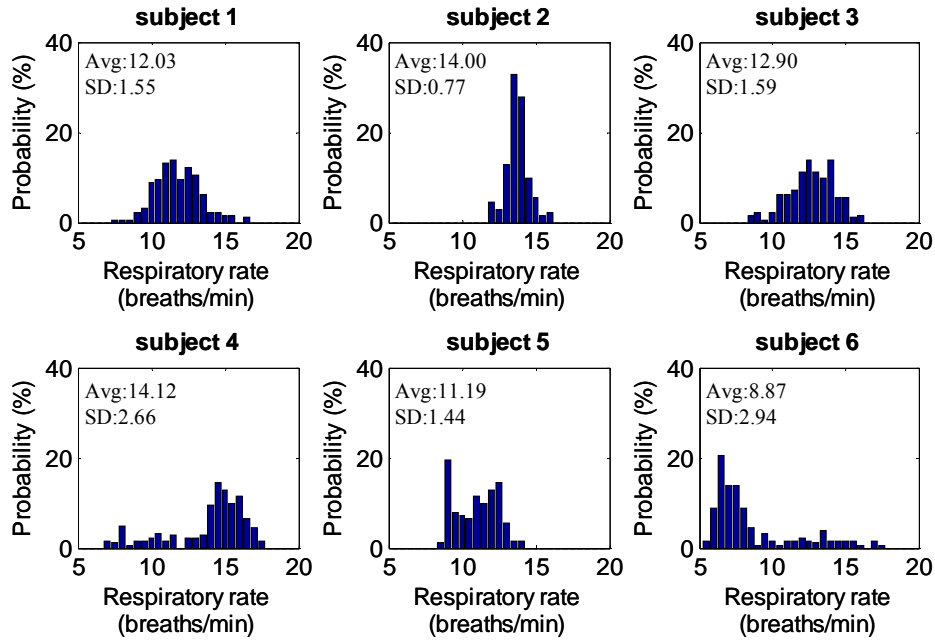


Fig 4.6 RR histograms for each meditation practitioner during the entire Chan-meditation course.

Fig 4.7 shows the HR (heart-rate) histograms for each experimental subject. Subjects #1, #2, and #4 had slower heart beating (<70 beats per minute, or bpm), while subject #4 had a much faster heart rate (>85 bpm) during the 30-minute Chan-meditation course. Heart rates of subjects #3 and #5 were in the normal range. Interestingly, subject #6 had the slowest breathing, yet fastest heart rate in the group. However, heart rate below 100 bpm is still within the normal range (in cardiology, a resting heart rate exceeding 100 bpm is considered to be under the risk of tachycardia for adults). In general, the body homeostasis during exercise makes the respiration faster (because more oxygen is needed) and simultaneously increases the heart rate to efficiently transport oxygen to the cells. In the study of Chan-meditation practitioners, we have observed such phenomenon as faster heart rate accompanying slower breathing, that will be further investigated in the future study.

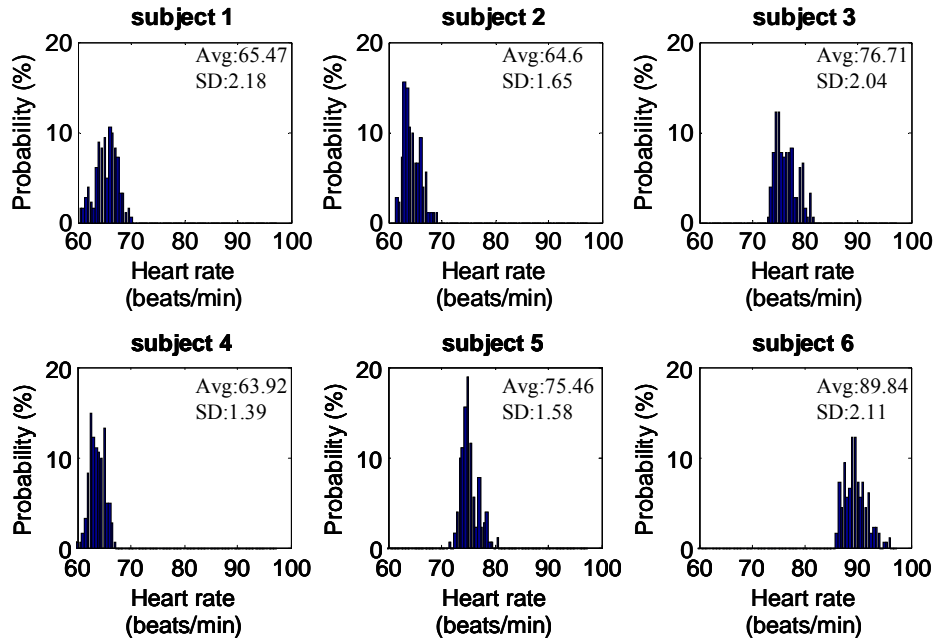


Fig 4.7 Heart-rate histograms for each meditation practitioner during the entire Chan-meditation course.

Fig 4.8 displays the $dps(\gamma)$ histograms for each meditation practitioner during the entire Chan-meditation course. We may clearly notice, from the histograms skewing towards the right side and higher value range of γ , that experimental subjects #3 and #5 had better cardiorespiratory phase synchronization. In fact, Fig 4.5 also reflects the bright grays dominating the 30-minute meditation course for these two subjects.

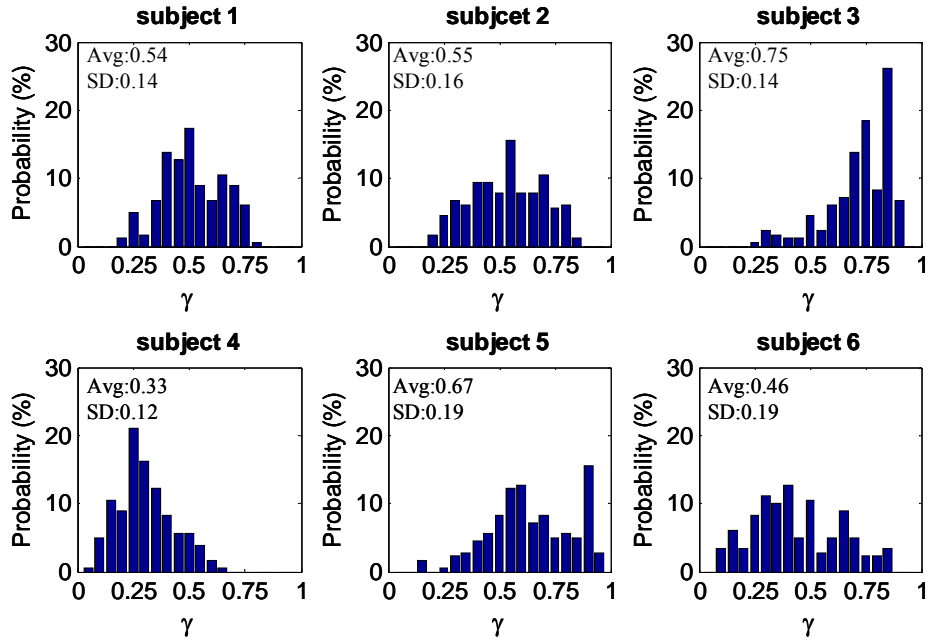


Fig 4.8 The dps (γ) histogram for each meditation practitioner during the entire Chan-meditation course.

Without pre-designed control factors like the RR used in the control experiment, we aim to interpret the results by classifying the data according to three RR ranges: slow, medium and fast breathing. As described in Section 3.3, there are 180 output samples in the 30-minute record based on 1-minute window size and 10-second moving step. We first sort the 180 RR samples in ascending order and then divide them into three equal sections, each containing 60 samples. Table 4.1 lists the resultant RR ranges of slow, medium, and fast breathing for each individual subject. Then, we are ready to investigate the cardiorespiratory phase synchronization under different RR's (as the control factor).

Table 4.1 RR ranges of slow, medium, and fast breathing for each individual subject in the experimental group (Chan-meditation practitioners).

	Respiratory rate (breaths / min)		
	slow	medium	fast
Subject 1	8~11	11~13	13~17
Subject 2	12~13	13~15	15~17
Subject 3	8~12	12~14	14~17
Subject 4	7~14	14~16	16~18
Subject 5	8~10	10~12	12~15
Subject 6	5~7	7~9	9~18

※ RR ranges 5~7 means $5 \leq \text{rate} < 7$

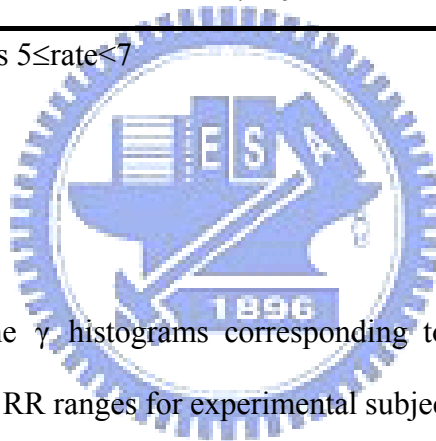
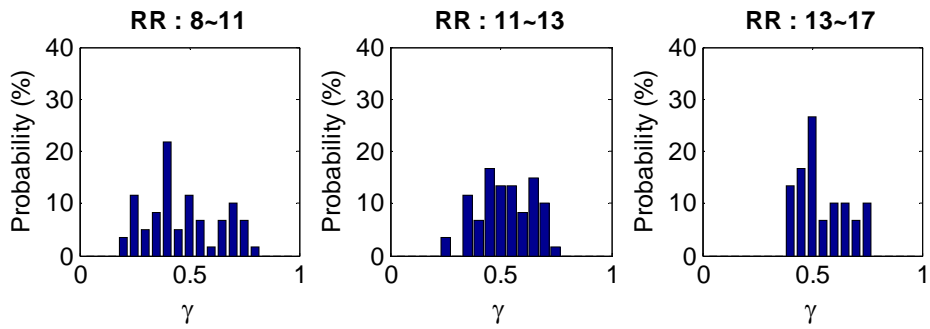
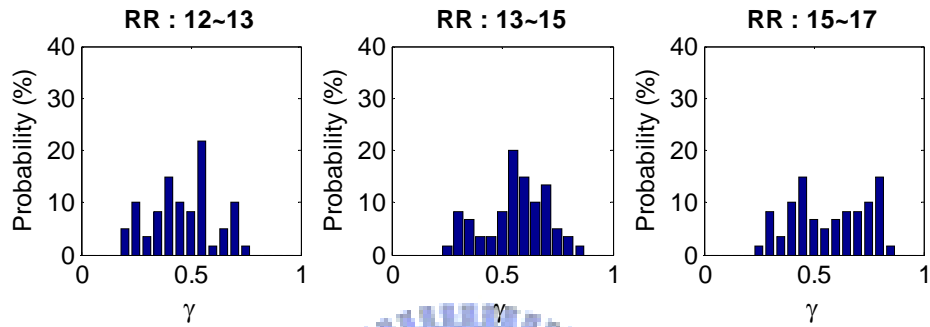


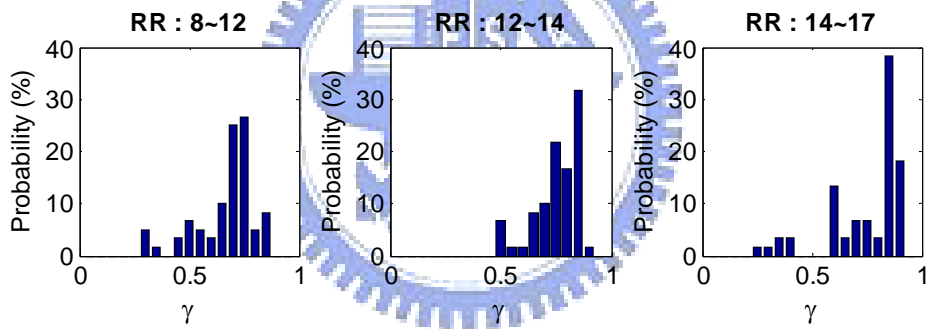
Fig 4.9 displays the γ histograms corresponding to the slow (left), medium (middle), and fast (right) RR ranges for experimental subjects #1 to #6 in figures (a) to (f). Based on eye-ball examination, we cannot tell any significant distinction of γ values among the three RR ranges for each individual. With the bar-chart illustration of average and standard deviation of γ values in each RR range (Fig 4.10), there still exists no statistically consistent indication like what observed in control group with breathing control.



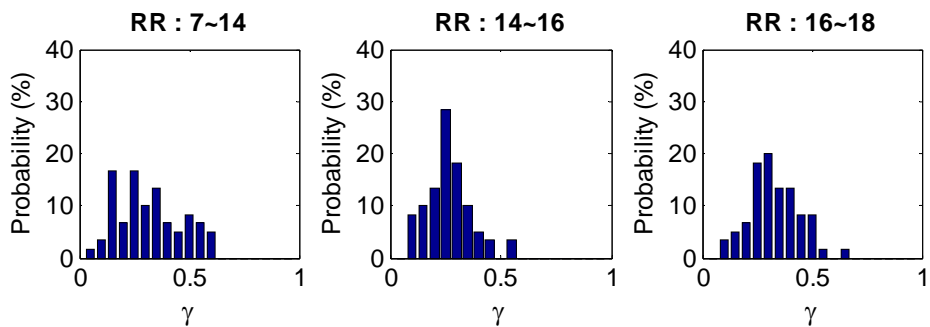
(a) experimental subjects #1



(b) experimental subjects #2

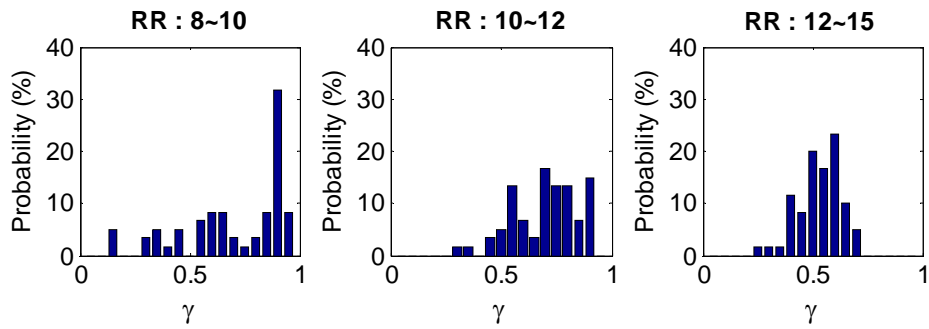


(c) experimental subjects #3

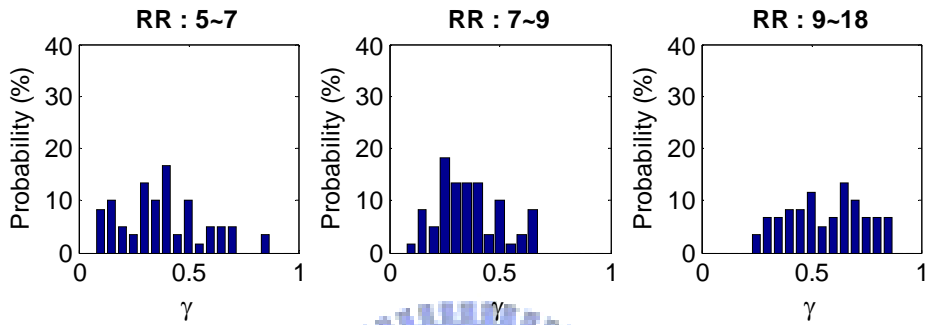


(d) experimental subjects #4

Fig 4.9 The γ histograms corresponding to the slow (left), medium (middle), and fast (right) respiratory ranges for experimental subjects #1 to #6 in (a) to (f).



(e) experimental subjects #5



(f) experimental subjects #6

Fig 4.9 (continue).

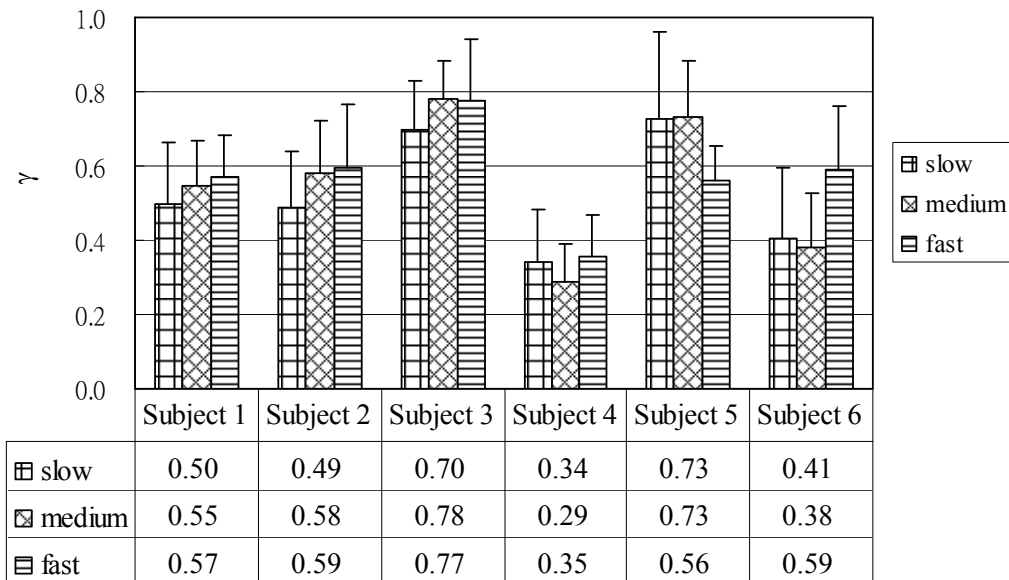
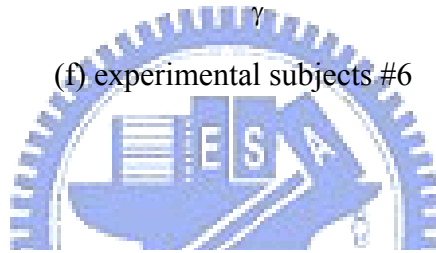


Fig 4.10 Bar-chart illustration of the average and std of γ values in the slow, medium, and fast RR ranges for each experimental subject

To eliminate the bias of different RR ranges among six experimental subjects, we further grouped the γ values according to the same RR ranges (slow: 9-11, medium: 12-14, and fast: 15-17 breaths/min). Then the group size (number of samples in each group) would be different, as shown in Table 4.2, due to the inter-subject variation.

Table 4.2 Number of samples within each RR range for all six experimental subjects under 30-minute Chan meditation (totally, 180 samples).

	Respiratory rate(breaths/min)		
	9-11	12-14	15-17
subject 1	43	69	8
subject 2	0	95	17
subject 3	20	83	15
subject 4	16	13	74
subject 5	74	62	0
subject 6	11	16	7

Table 4.3 list the average and standard-deviation (SD) results of γ values in each RR group. The RR range of 9-11 breaths/min does not show any preference for the average γ , which is even the smallest for subjects #1, #3, #4, and #6. As the results quite conflict with what obtained in the control group, we hypothesize that the major cause might be due to the inconsistency of respiratory rate during meditation. When meditating freely, Chan-meditation practitioners may breathe at a rate changing from time to time. Is there any requirement of the shortest duration of consistent slow breathing (at 10 breaths/min) in order to achieve an enhanced cardiorespiratory phase synchronization? We will leave this issue to the future study.

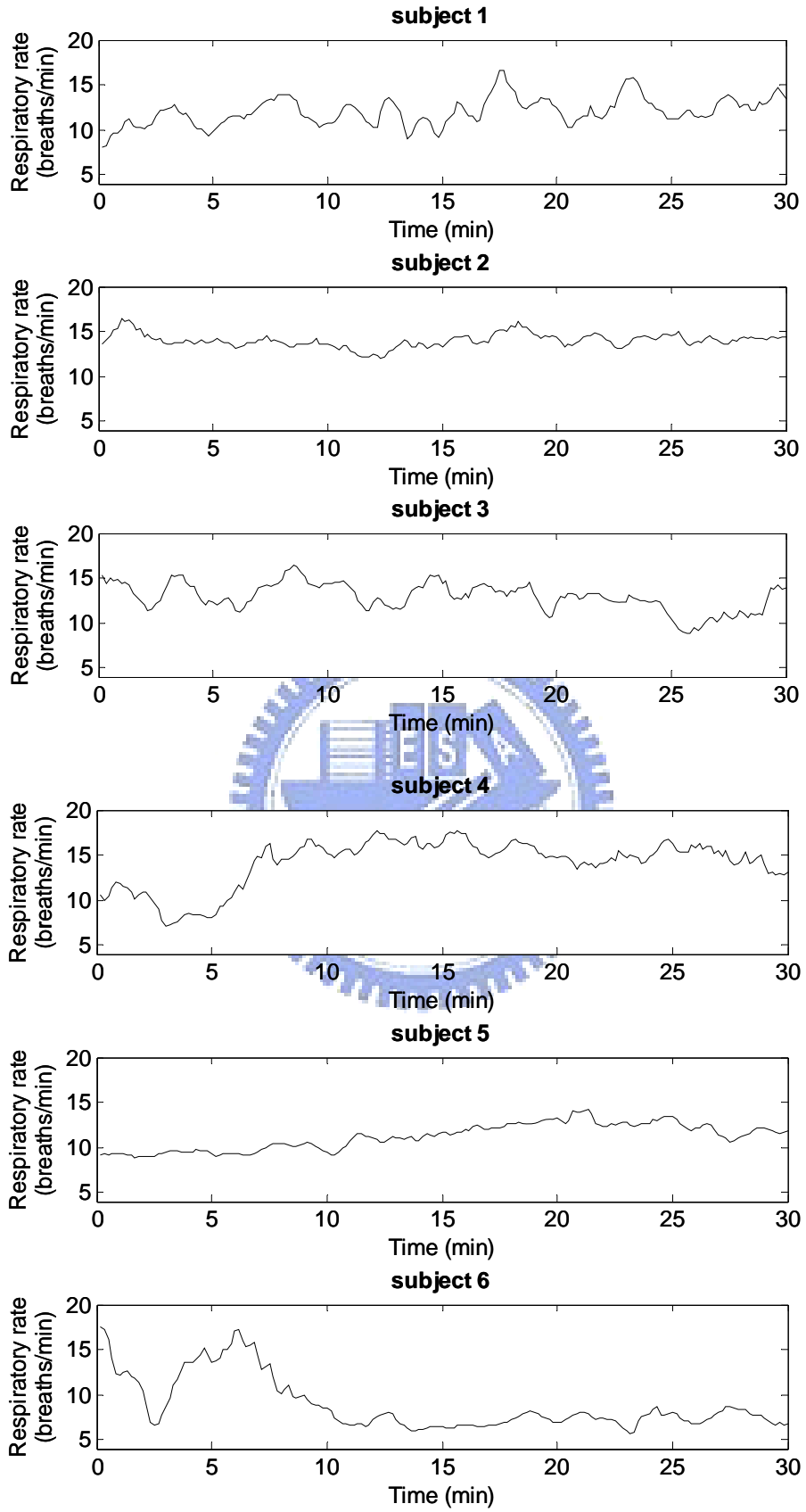
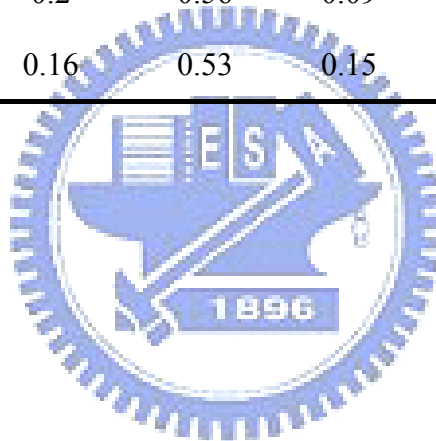


Fig 4.11 The time-dependent Respiratory rate for experimental subject.

Table 4.3 The average and std of γ values in the group of slow (9-11), medium (12-14), and fast (15-17) RR ranges.

	Respiratory rate (breaths/min)					
	9-11		12-14		15-17	
	Average	SD	Average	SD	Average	SD
subject 1	0.52	0.18	0.56	0.11	0.61	0.12
subject 2	0	0	0.51	0.14	0.41	0.09
subject 3	0.65	0.15	0.77	0.11	0.75	0.19
subject 4	0.28	0.12	0.44	0.14	0.32	0.12
subject 5	0.77	0.2	0.56	0.09	0	0
subject 6	0.44	0.16	0.53	0.15	0.73	0.06



4.3 Overall comparison between two groups

For the lump-sum comparison between two groups, we first make a plot for the histogram of RR samples of all six subjects in the control (Fig 4.12) and experimental (Fig 4.13) group. The RR-dependent γ analysis was conducted for four RR ranges: <8 , 8-12, 12-16, and >16 breaths/min. Figs 4.14 and 4.15 illustrate respectively the γ distributions for the control and the experimental group.

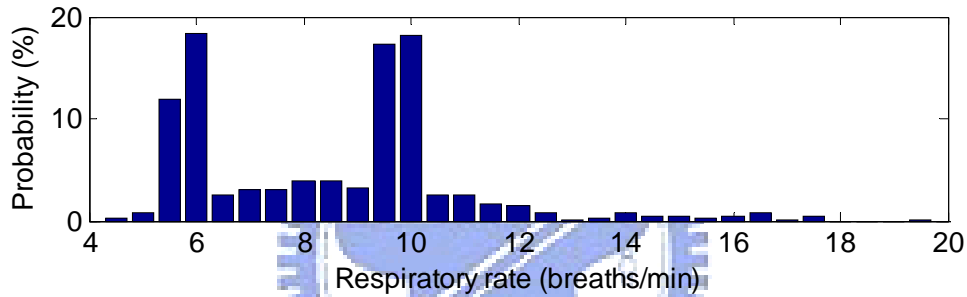


Fig 4.12 RR histogram for all the control subjects. There will be totally $180 \times 6 = 1080$ R samples.

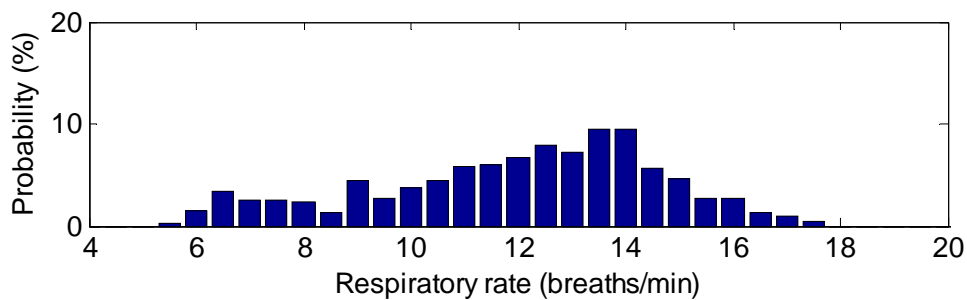


Fig 4.13 RR histogram for all the experimental subjects (1080 RR samples overall).

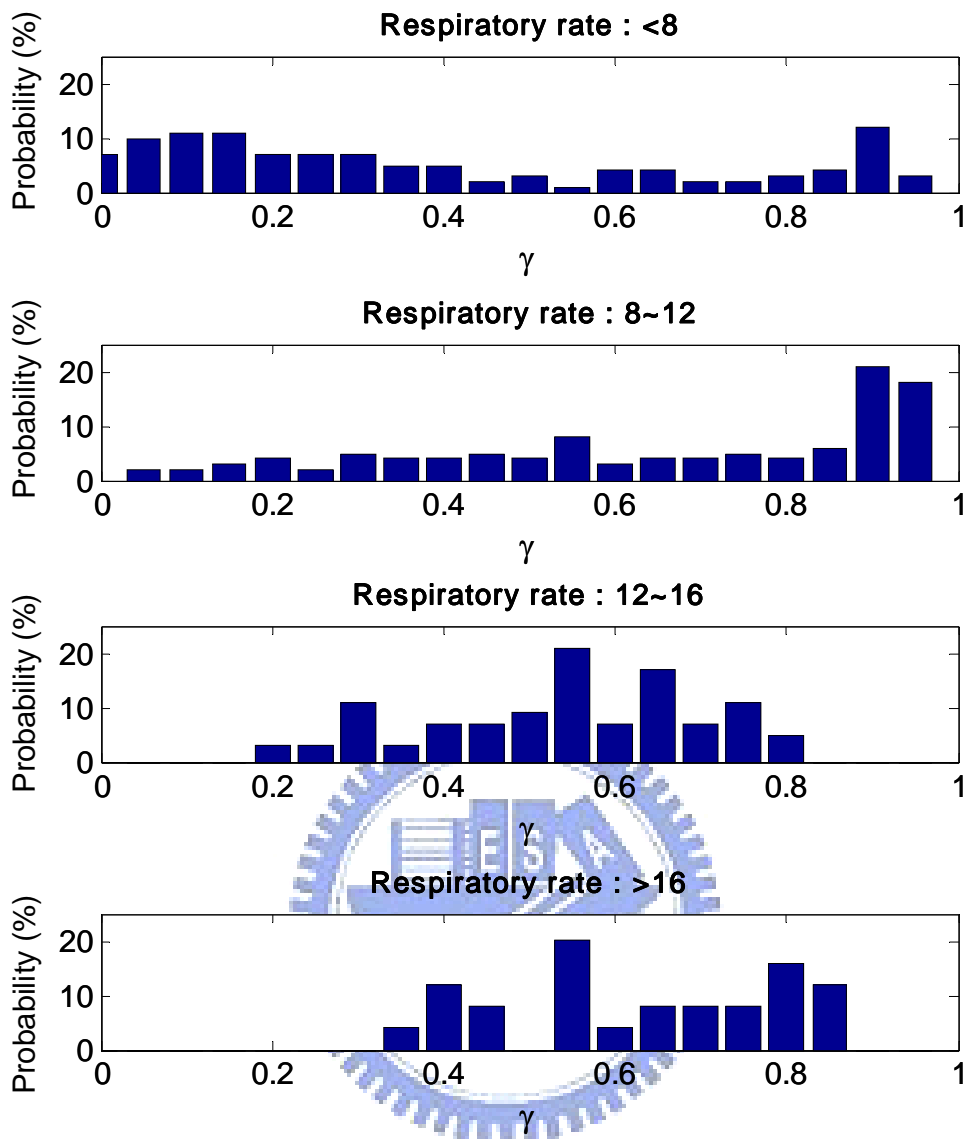


Fig 4.14 The γ distributions with the RR in the range (from the top): <8, 8-12, 12-16, and >16 breaths/min for the control group.

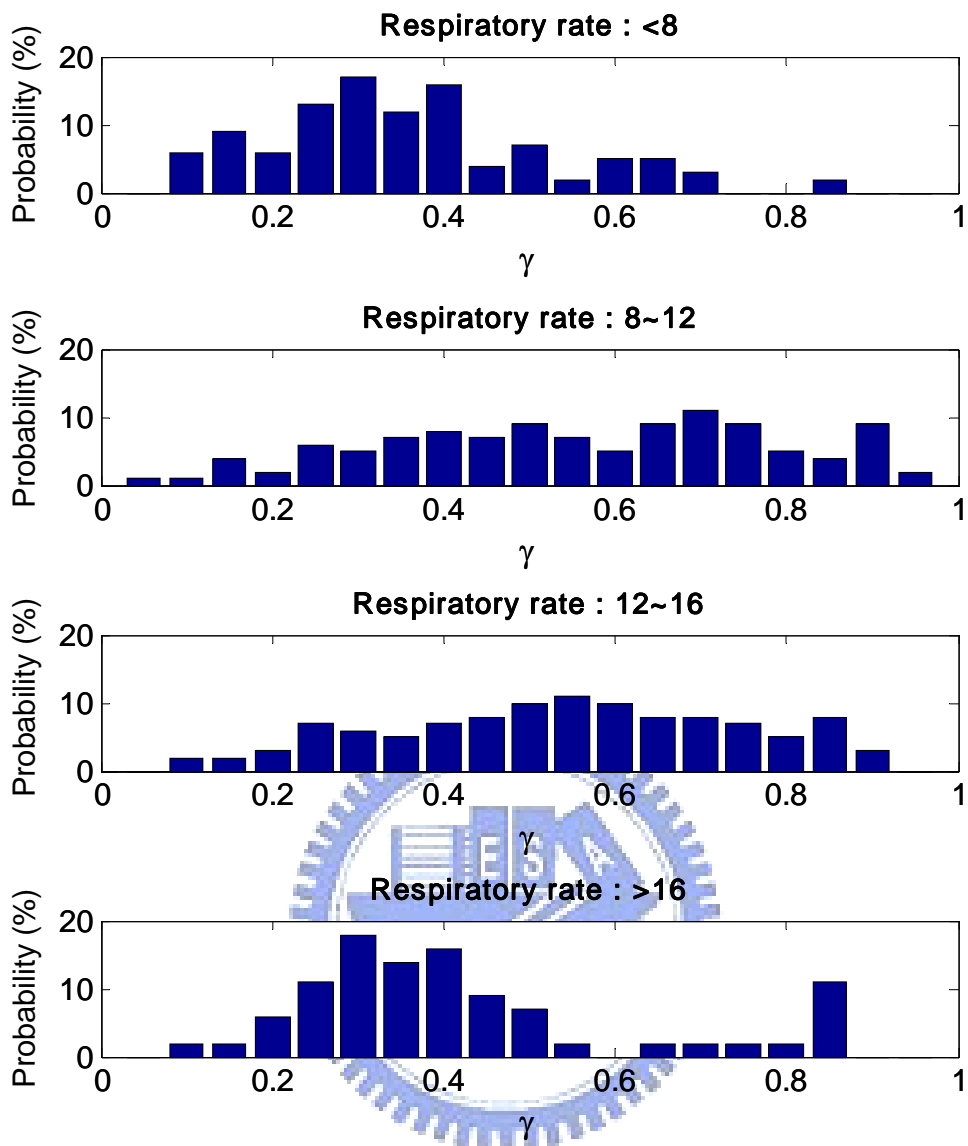


Fig 4.15 The γ distributions with the RR in the range (from the top): <8, 8-12, 12-16, and >16 breaths/min for the experimental group.

Fig 4.14 apparently reflects the better cardiorespiratory phase synchronization for the control group with breathing rate regulated at 10 breaths/min, under the guide of audio cue. Besides, the γ values concentrate mostly in the range of 0.4 – 0.8 when RR is in both the 12-16 and >16 breaths/min, belonging to the normal RR for healthy adults. While meditation practitioners breathing at the rate of either slower than 8 or faster than 16 breaths/min, they exhibit poorer cardiorespiratory phase synchronization ($\gamma < 0.5$, Fig 4.15). From both the average and SD values listed in Table 4.4 and the tendency

plot in Fig 4.16, we may draw preliminary conclusions as follows

1. On average, this experimental group had poorer cardiorespiratory phase synchronization than the control group.
2. Both groups consistently reveal the effect of worse synchronization when breathing at the rate slower than 8 breaths/min.
3. Faster breathing with $RR > 16$ breaths/min results in the opposite effect on the control and the experimental group.

Table 4.4 Average and standard deviation of γ values in the group of RR's: <8, 8-12, 12-16, and >16 breaths/min for the control and the experimental group.

	Respiratory Rate (breaths/min)							
	<8		8-12		12-16		>16	
	Average	SD	Average	SD	Average	SD	Average	SD
Control Group	0.4	0.31	0.7	0.26	0.57	0.15	0.65	0.16
Experimental Group	0.38	0.16	0.59	0.22	0.57	0.19	0.45	0.19

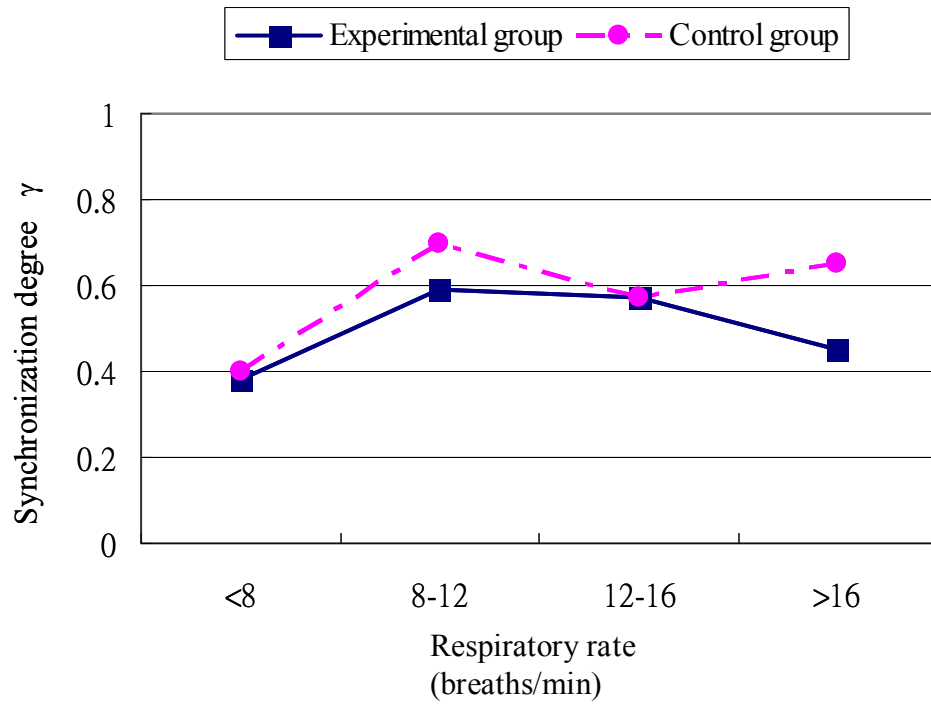
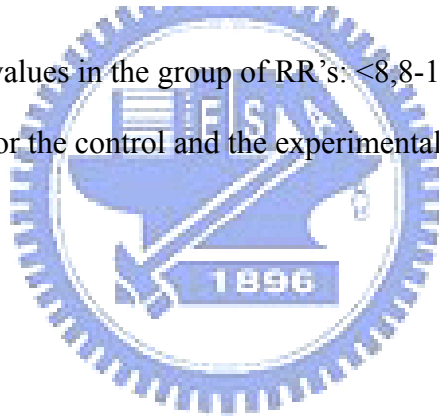


Fig 4.16 Average of γ values in the group of RR's: <8, 8-12, 12-16, and >16 breaths/min for the control and the experimental group.



Chapter 5

Conclusion and Discussion

5.1 Conclusion and Discussion

In this thesis, we studied the cardiorespiratory interaction scheme based on the analysis of instantaneous phases of heart-rate time series and raw respiratory signal.

Like almost all natural phenomena, HRV is the result of many nonlinearly interacting processes; therefore any linear analysis has the potential risk of underestimating, or even missing, a great amount of information content. Recently the Empirical Mode Decomposition (EMD), a signal processing technique particularly suitable for nonlinear and nonstationary series, has been proposed as a new tool for data analysis. This technique performs a time adaptive decomposition of a complex signal into elementary, almost orthogonal components that do not overlap in frequency. The extracted components have well behaved Hilbert transforms, from which the instantaneous phase can be calculated. Accordingly, we applied the instantaneous phase analysis based on Hilbert-Huang Transform (HHT) to our study of cardiorespiratory interaction properties for Chan-meditation practitioners and controls

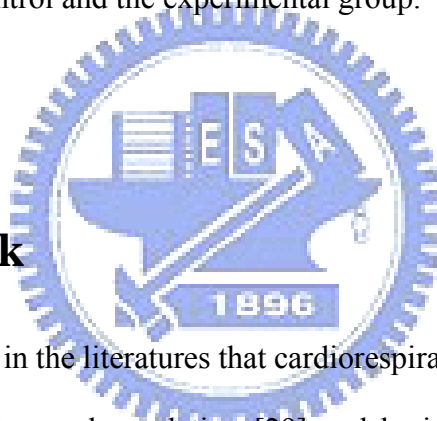
The results for control subject, The gray-level monochrome image in Fig 4.2 illustrates the temporal evolution of γ for all the control subjects, with brighter gray corresponding to larger γ . All subjects exhibit consistently higher γ in the 2nd session, that is further confirmed by the highest average *dps* in Fig 4.3.

The results for experimental subject quite conflict with what obtained in the control group, we hypothesize that the major cause might be due to the inconsistency of respiratory rate during meditation. When meditating freely, Chan-meditation practitioners may breathe at a rate changing from time to time.

For the lump-sum comparison between two groups, we may draw preliminary conclusions as follows: (1) On average, this experimental group had poorer cardiorespiratory phase synchronization than the control group. (2) Both groups consistently reveal the effect of worse synchronization when breathing at the rate slower than 8 breaths/min. (3) Faster breathing with $RR > 16$ breaths/min results in the opposite effect on the control and the experimental group.

5.2 Future Work

It has been reported in the literatures that cardiorespiratory synchronization might be related to the central neural regulation [29] and brain activity [10]. Hence, for profound understanding of the Zen-meditation process and effects, EEG signals should be included to explore the mutual interaction between the brain and cardiorespiratory system. For example, analysis of heart rate variability could reflect the influence of autonomic nervous system.



Reference

- [1] R. Sudsuang, V. Chentanez, and K. Veluvan, "Effect of buddhist meditation on serum cortisol and total protein levels, blood pressure, pulse rate, lung volume and reaction time," *Physiology & Behavior*, vol. 50, 1991, pp. 543-548.
- [2] C.R.K. MacLean, K.G. Walton, S.R. Wenneberg, D.K. Levitsky, J.P. Mandarino, R. Waziri, S.L. Hillis, and R.H. Schneider, "Effects of the transcendental meditation program on adaptive mechanisms: Changes in hormone levels and responses to stress after 4 months of practice," *Psychoneuroendocrinology*, vol. 22, 1997, pp. 277-295.
- [3] R. Davidson, J. Kabat-Zinn, J. Schumacher, M. Rosenkranz, D. Muller, S. Santorelli, F. Urbanowski, A. Harrington, K. Bonus, and J. Sheridan, "Alterations in brain and immune function produced by mindfulness meditation," *PSYCHOSOMATIC MEDICINE*, vol. 65, Aug. 2003, pp. 564-570.
- [4] S. Lazar, C. Kerr, R. Wasserman, J. Gray, D. Greve, M. Treadway, M. McGarvey, B. Quinn, J. Dusek, H. Benson, S. Rauch, C. Moore, and B. Fischl, "Meditation experience is associated with increased cortical thickness," *NEUROREPORT*, vol. 16, Nov. 2005, pp. 1893-1897.
- [5] C. Liu and P. Lo, "Investigation of spatial characteristics of meditation EEG using wavelet analysis and fuzzy classifier," *PROCEEDINGS OF THE FIFTH IASTED INTERNATIONAL CONFERENCE ON BIOMEDICAL*, 2007, pp. 91-96.

- [6] H. Huang and P. Lo, "EEG dynamics of experienced Zen meditation practitioners probed by complexity index and spectral measure," *Journal of Medical Engineering & Technology*, vol. 33, 2009, pp. 314-321.
- [7] C. Liu, C. Wei, and P. Lo, "Variation Analysis of Sphygmogram to Assess Cardiovascular System under Meditation," *eCAM*, 2007, pp. nem065.
- [8] F. Raschke, "The respiratory system—Features of modulation and coordination," In: Haken H, Koepchen HP (ed) *Rhythms in physiological systems*, Springer, Berlin, 1991.
- [9] E. Toledo, S. Akselrod, I. Pinhas, and D. Aravot, "Does synchronization reflect a true interaction in the cardiorespiratory system?," *Medical Engineering & Physics*, vol. 24, 2002, pp. 45-52.
- [10] R. Bartsch, J.W. Kantelhardt, T. Penzel, and S. Havlin, "Experimental Evidence for Phase Synchronization Transitions in the Human Cardiorespiratory System," *Physical Review Letters*, vol. 98, 2007, pp. 054102.
- [11] D.C. Galletly and P.D. Larsen, "Cardioventilatory coupling during anaesthesia," *Br. J. Anaesth.*, vol. 79, 1997, pp. 35-40.
- [12] A. Stefanovska, H. Haken, P.V.E. McClintock, M. Hozcaronicaron, F. Bajrovicacuta, and S. Ribariccaron, "Reversible Transitions between Synchronization States of the Cardiorespiratory System," *Physical Review Letters*, vol. 85, 2000, pp. 4831.
- [13] P. Lo and S. Wu, "Effect of Zen Meditation Practice on Perceived Stress in College Students: a Survey Study," *Biomedical Engineering: Applications, Basis and Communications*, vol. 19, 2007, pp. 409.

- [14] N. Goldschlager, *Principles of Clinical Electrocardiography*, Appleton & Lange, 1989.
- [15] P. Flandrin, *Time-frequency/time-scale analysis*, Academic Press, 1999.
- [16] K. Gröchenig, *Foundations of time-frequency analysis*, Birkhäuser, 2001.
- [17] H. Kantz and T. Schreiber, *Nonlinear time series analysis*, Cambridge University Press, 2004.
- [18] H. Tong, *Non-linear time series: a dynamical system approach*, Oxford University Press, 1993.
- [19] N.E. Huang and S.S. Shen, *The Hilbert-Huang Transform and Its Applications*, World Scientific Publishing Company, 2005.
- [20] N.E. Huang, Z. Shen, S.R. Long, M.C. Wu, H.H. Shih, Q. Zheng, N. Yen, C.C. Tung, and H.H. Liu, "The Empirical Mode Decomposition and the Hilbert Spectrum for Nonlinear and Non-Stationary Time Series Analysis," *Proceedings: Mathematical, Physical and Engineering Sciences*, vol. 454, March. 1998, pp. 903-995.
- [21] M.G. Rosenblum, A.S. Pikovsky, and J. Kurths, "Phase Synchronization of Chaotic Oscillators," *Physical Review Letters*, vol. 76, 1996, pp. 1804.
- [22] M.G. Rosenblum, A.S. Pikovsky, and J. Kurths, "From Phase to Lag Synchronization in Coupled Chaotic Oscillators," *Physical Review Letters*, vol. 78, 1997, pp. 4193.

- [23] D. Gabor, "Theory of communication. Part 1: The analysis of information," *Electrical Engineers - Part III: Radio and Communication Engineering, Journal of the Institution of*, vol. 93, 1946, pp. 429-441.
- [24] R. Mrowka, A. Patzak, and M. Rosenblum, "Quantitative Analysis of Cardiorespiratory Synchronization in Infants," 2000.
- [25] P. Tass, M.G. Rosenblum, J. Weule, J. Kurths, A. Pikovsky, J. Volkmann, A. Schnitzler, and H. Freund, "Detection of n:m Phase Locking from Noisy Data: Application to Magnetoencephalography," *Physical Review Letters*, vol. 81, 1998, pp. 3291.
- [26] D. Cysarz, D. von Bonin, H. Lackner, P. Heusser, M. Moser, and H. Bettermann, "Oscillations of heart rate and respiration synchronize during poetry recitation," *Am J Physiol Heart Circ Physiol*, vol. 287, 2004, pp. H579-587.
- [27] D. Cysarz and A. Büssing, "Cardiorespiratory synchronization during Zen meditation," *European Journal of Applied Physiology*, vol. 95, 2005, pp. 88-95.
- [28] R. Balocchi, D. Menicucci, E. Santarcangelo, L. Sebastiani, A. Gemignani, B. Ghelarducci, and M. Varanini, "Deriving the respiratory sinus arrhythmia from the heartbeat time series using empirical mode decomposition," *Chaos, Solitons & Fractals*, vol. 20, 2004, pp. 171-177.
- [29] C. Schäfer, M.G. Rosenblum, H. Abel, and J. Kurths, "Synchronization in the human cardiorespiratory system," *Physical Review E*, vol. 60, 1999, pp. 857.

Appendix A

R Peak and Respiratory Peak Detections

I.1 R Peak Detection

The flow chart of R peak detection is shown in Fig. A.1. Original ECG signal that is digitized at 1000Hz is resampled to 200 Hz using Matlab's built-in polyphase filter implementation, including anti-aliasing (lowpass) FIR filter. Then the bandpass filter 10~30 Hz is used to reduce the influence of muscle noise, 60Hz interference, baseline drift, and T-wave interference. R peaks are strengthened by $x(n) * |x(n)|$. As shown in Fig. A.2, the ECG signal before and after preprocessing is presented, and the amplitude of R waves are obviously revealed. Because the amplitude of ECG signal is different from one to another, and there also exists difference amplitude for the same subject, thus the setting of a threshold must be adaptive so that R peak won't be missed or judged incorrectly. Therefore we use 1 minute moving window, and the threshold is determined by $0.3 * \text{maximum value in the window}$. From the above, we could detect the time position of R peak from ECG signal for further study.

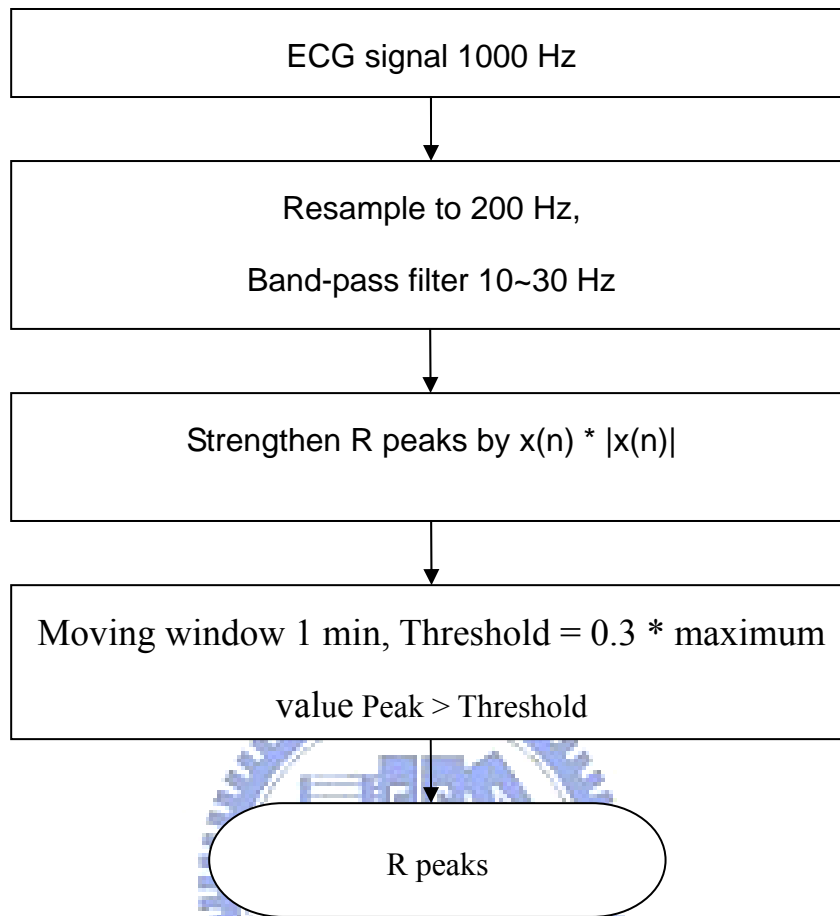


Fig. A.1 Flow chart of R peak detection

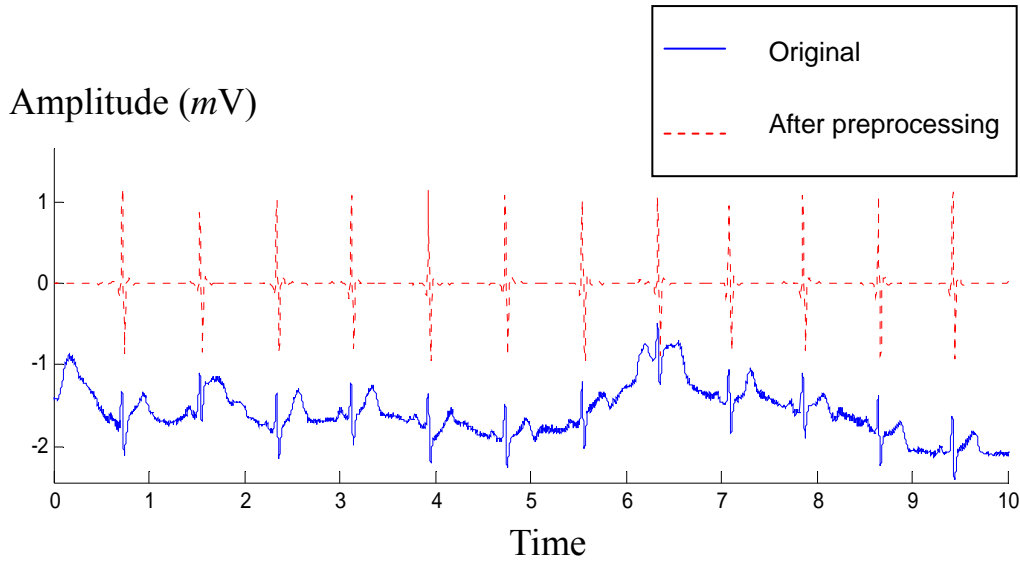


Fig. A.2 ECG after preprocessing

I.2 Respiratory Peak Detection

The flow chart of Respiratory peak detection is shown in Fig. A.3. Original Respiratory signal that is digitized at 1000 Hz is resampled to 20 Hz using Matlab's built-in polyphase filter implementation, including anti-aliasing (lowpass) FIR filter. Then the bandpass filter 0.1~0.45 Hz is used to reducing the influence of baseline drift, and the main energy of respiratory signal is in this frequency range in this study. As shown in Fig. A.4, the respiratory signal before and after preprocessing is presented. In Fig. A.5, the parameters of normalized respiratory signal after preprocessing are shown, where t_k is the time position of k_{th} respiratory peak, d_{up} is the amplitude of inspiration, and d_{down} is the amplitude of expiration. The conditions of d_{up} and $d_{down} > 0.05$ and the peak value at time $t_k > 0$ is considered to determine the time position of respiratory signal for further study.

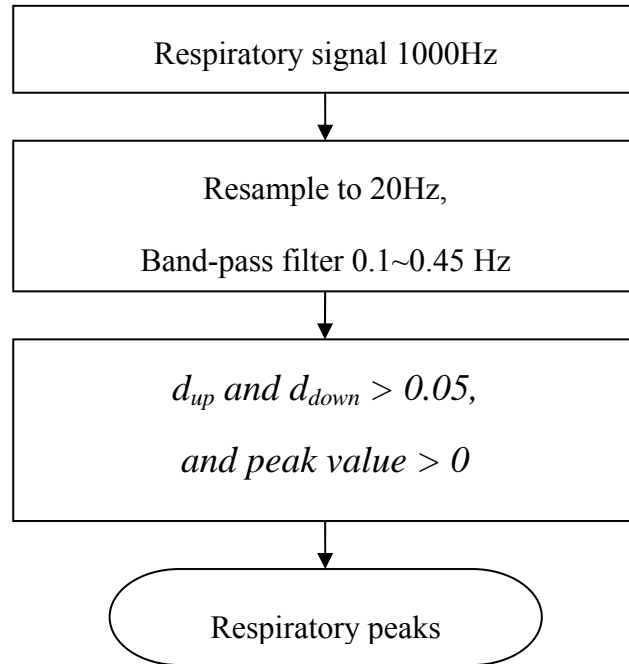


Fig. A.3 Flow chart of Respiratory peak detection

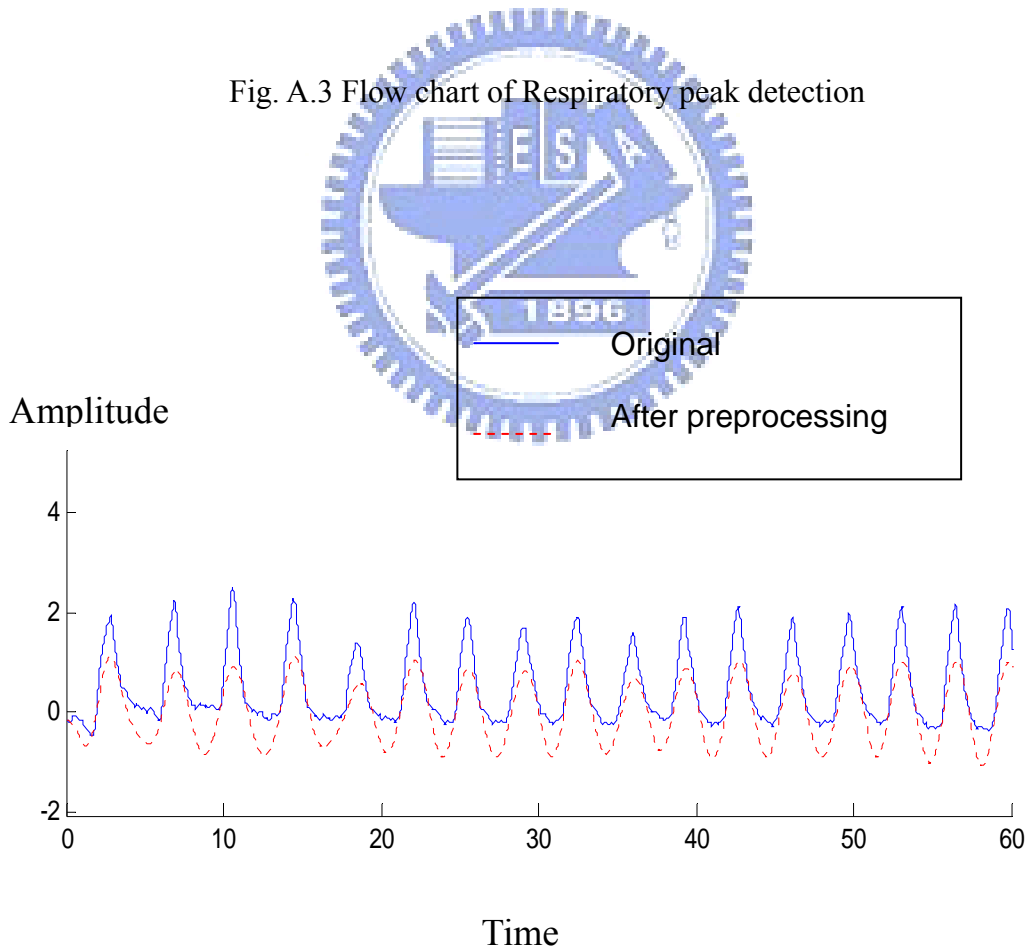


Fig. A.4 Respiratory signal after preprocessing

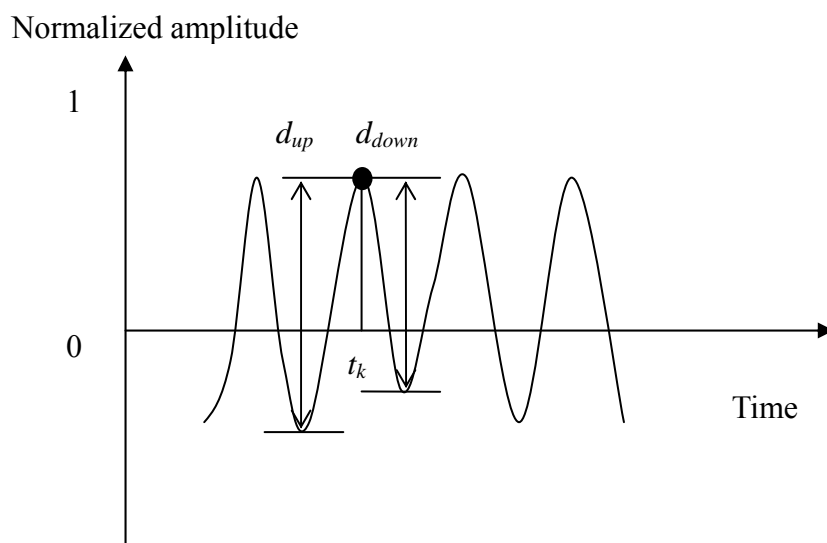


Fig. A.5 The parameters of respiratory signal



Appendix B

Formal Chan-meditation Practice

Formal Chan-meditation course normally begins with a brief, solemn ritual called 開經偈 signifying “the opening ceremony of the practice towards complete enlightenment.” In the next 5-10 minutes, the class supervisor (normally, the experienced practitioner) shares wisdom words preached by the enlightened Chan Master, Wu Chueh Miao Tien, the 85th patriarch of orthodox Dharma-Chan sect. Meanwhile, practitioners sit calmly with meditation posture and belly breathing, yet, eyes opening.

Then, formal Chan-meditation session begins. In the beginning meditation, practitioners focus on particular chakras to activate the intrinsic potency and wisdom of those chakras. Gradually, the entire body-mind-spirit enters into a field of harmony after transcending the physical, mental, emotional and conscious realm. The goal of Chan meditation is to realize the *True Self* with eternal wisdom.

After the meditation session, practitioners open eyes and listen to the sharing from the supervisor for about ten more minutes. Then, the class ends with a brief closing ritual and the chanting of *The Song of True Self*.

Appendix C

Continuous Hilbert transform

$$\mathcal{H}\{g(t)\} = g(t) * \frac{1}{\pi t} = \frac{1}{\pi} \int_{-\infty}^{\infty} \frac{g(\tau)}{t - \tau} d\tau \quad (\text{C.1})$$

The Hilbert transform of $g(t)$ is the convolution of $g(t)$ with the signal $1/(\pi t)$. It is the response of a linear time-invariant filter (called a Hilbert transformer) with impulse response $1/(\pi t)$, given an input $g(t)$.

Gabor introduced the analytic signal as a signal without negative frequencies [23]. Based on Gabor's definition, the analytic counterpart of the real signal, $g(t)$, can be obtained by suppressing the negative frequencies of the spectrum. The analytic signal, $z(t)$, of the real signal $g(t)$ is given by:

$$z(t) = a(t) \cdot e^{j\phi(t)} = g(t) + \frac{j}{\pi} \int_{-\infty}^{\infty} \frac{g(\tau)}{t - \tau} d\tau = g(t) + j\hat{g}(t) \quad (\text{C.2})$$

where $\hat{g}(t)$ is the Hilbert transform of $g(t)$. The amplitude $a(t)$ and instantaneous phase $\phi(t)$ are defined by:

$$a(t) = \sqrt{g^2(t) + \hat{g}^2(t)} \quad (\text{C.3})$$

$$\phi(t) = \tan^{-1} \left(\frac{\hat{g}(t)}{g(t)} \right) \quad (\text{C.4})$$

The instantaneous frequency is defined as the rate of phase change:

$$\omega(t) = \frac{d\phi(t)}{dt} \quad (\text{C.5})$$

Then, the instantaneous phase and instantaneous frequency are ready to be estimated based on Eqs. (C.4) and (C.5).